~~CONFIDENTIAL~~

RM A55G13

NACA RM A55G13

NACA

RESEARCH MEMORANDUM

AN INVESTIGATION OF THE EFFECTS OF NOSE AND LIP SHAPES FOR AN UNDERSLUNG SCOOP INLET AT MACH NUMBERS FROM 0 TO 1.9

By Frank A. Pfyl

Ames Aeronautical Laboratory
Moffett Field, Calif.

[redacted]

NATIONAL ADVISORY COMMITTEE
FOR AERONAUTICS

WASHINGTON

November 18, 1955

[redacted]

NACA RM A55G13

NATIONAL ADVISORY COMMITTEE FOR AERONAUTICS

RESEARCH MEMORANDUM

AN INVESTIGATION OF THE EFFECTS OF NOSE AND LIP SHAPES FOR AN UNDERSLUNG SCOOP INLET AT MACH NUMBERS FROM 0 TO 1.9

By Frank A. Pfyl

SUMMARY

An experimental investigation was conducted to determine the performance characteristics of an underslung nose-scoop air-induction system for a supersonic airplane. Five different nose shapes, three lip shapes, and two internal diffusers were investigated. Tests were made at Mach numbers from 0 to 1.9, angles of attack from 0° to approximately 15°, and mass-flow ratios from 0 to maximum obtainable.

It was found that the underslung nose-scoop inlet was able to operate at Mach numbers from 0.6 to 1.9 over a large positive angle-of-attack range without adverse effects on the pressure recovery. Although there was no one inlet configuration that was markedly superior over the entire range of operating variables, the arrangement having a nose designed to give increased supersonic compression at low angles of attack, and a sharp lip (configuration designated N_3L_3) showed the most favorable performance characteristics over the supersonic Mach number range. Inlets with sizable lip radii gave satisfactory performance up to a Mach number of 1.5; however, as a result of an increase in drag, the performance of such inlets was markedly inferior to the sharp-lip configuration above Mach numbers of 1.5.

Throughout the range of test Mach numbers all inlet configurations evidenced stable air-flow characteristics over the mass-flow range for normal engine operation.

Analysis of the inlet performance on the basis of a propulsive thrust parameter showed that a fixed inlet area could be used for Mach numbers up to 1.5 with only a small sacrifice in performance.

Author

INTRODUCTION

In selecting an air-induction system for a high-speed interceptor airplane having the engine located within the fuselage, the designer generally has the choice of side-scoop or nose air inlet systems. For the particular design problem where the radar scanning equipment is a necessary component of the airplane, the placement of the inlet in the compression field of the radome nose can be advantageous. Several underslung inlet studies have shown that no serious adverse effects on pressure recovery occur at off-design positive angles of attack and that the problems associated with boundary-layer air are of secondary importance (see refs. 1 and 2).

When selecting a nose shape for an underslung scoop inlet, consideration must be given to the drag of the nose and inlet combination as well as the pressure recovery. Changing the length or roundness of the nose contours alters the flow field in the vicinity of the inlet, thereby affecting the pressure recovery of the inlet and the drag of the body in the region of the inlet. On such installations the drag increment due to changing the nose contour may be considered to have two components; the drag increment of the nose itself, and the drag increment due to the altered flow field in the lip region of the inlet. To evaluate the effect of nose shape on the performance of an underslung inlet installation, five nose shapes of different nose contours and fineness ratios were investigated for one lip location. Also, three lip shapes to compare the differences between rounded- and sharp-lip profiles were tested. Measurements were made of mass-flow ratio, pressure recovery, drag, and air-flow stability over a wide range of operating variables. The performance of the most favorable nose and lip combinations are compared analytically by means of a propulsive thrust parameter. The investigation was conducted in the Ames 6- by 6-foot supersonic wind tunnel at Mach numbers of 0 to 1.9.

NOTATION

A	area, sq ft
C_D	net drag coefficient, $\frac{D}{qS}$
D	net drag, lb
L	lip (used for lip designation)
L.E.R.	lip leading-edge radius
M	Mach number

m	mass flow through inlet, slugs/sec
$\frac{m_c}{m_\infty}$	ratio of the mass flow through the inlet to the mass flow at free-stream conditions passing through an area equal to the inlet entrance area, $\frac{\rho_c A_c V_c}{\rho_o A_i V_o}$
N	nose (used for nose designation)
N.S.	normal shock
p_t	total pressure, lb/sq ft
$\frac{p_{t_c}}{p_{t_\infty}}$	total pressure ratio at compressor station
q	dynamic pressure, lb/sq ft
R	Reynolds number (based on assumed MAC 0.94 ft)
S	assumed wing area, 375 sq ft
T_{isen}	net thrust with isentropic pressure recovery, lb
T_N	net thrust with measured pressure recovery, lb
V	velocity, ft/sec
$\frac{W_a\sqrt{\theta}/\delta}{A_i}$	air-flow parameter, lb/sec/sq ft
W_a	weight of air, lb/sec
α	angle of attack of fuselage reference axis, deg
β	angle of sideslip, deg
δ	engine station total pressure divided by NACA sea-level static pressure
η	propulsive thrust parameter, $\frac{T_N - D}{T_{isen}}$
θ	engine station absolute total temperature divided by NACA ambient sea-level temperature
ρ	mass density of air, slugs/cu ft

[redacted]

Subscripts

c	compressor station
i	inlet entrance station (lip leading edge)
∞	free-stream conditions

APPARATUS AND PROCEDURE

The partial model of a high-speed fighter airplane with an underslung nose inlet was sting-mounted in the Ames 6- by 6-foot supersonic wind tunnel. (See ref. 3 for information regarding the wind tunnel.) A drawing of the model is shown in figure 1. Five different nose shapes (resulting from two basic nose lengths), three lip shapes ranging from a sharp lip to a blunt lip, and two basic internal diffusers were investigated on the model. Each modification of the model has been given a number and these numbers will be referred to in the remainder of this report. For the long radome nose lengths three nose contours were investigated; a sharp nose, N_1, a rounded nose N_2, and a rounded nose with the slope of the lower surface increased to effectively generate greater compression, N_3. Two nose contours were tested with a short radome nose length; a sharp nose, N_4, and a rounded nose, N_5. Of the three lip profiles investigated the bluntest lip is designated L_1, the intermediate lip L_2, and the sharp lip L_3. The change made to the diffuser cross section, which relieved the internal contraction near the inlet entrance, was tested in conjunction with the sharp lip, L_3, only and is referred to in the text as L's. The basic configuration was considered to be the long rounded nose and intermediate lip N_2L_2. A comparison of various nose and lip combinations can be seen in the photographs of figure 2. Details of the nose shapes and lip profiles are given in figures 3 and 4 and tables 1 and 2. The area distributions of the internal diffusers are presented in figure 5, and figure 6 presents the model cross-sectional area.

Two survey rakes, one at the simulated compressor inlet, and the other near the model exit (see fig. 1) were used to measure the internal air-flow characteristics. The measurements from the survey rake at the compressor inlet were used to determine the total-pressure recovery and mass flow through the model. Prior to the wind-tunnel tests, a bench test calibration was made to establish a factor correlating the mass flow through the model as measured from the compressor inlet survey rakes with the mass flow through a standard ASME orifice meter. The calibration factor from these bench tests, and the integrated total and static pressures at the compressor inlet were used in obtaining the mass flow through the model for this investigation. The area-weighted total-pressure measurements from the survey rake near the model exit were used in calculating

the total momentum of the internal flow. The internal flow force is defined as the change in total momentum of the entering streamtube from the free stream to the exit of the model, and is thus consistent with the usual definition of jet-engine thrust. The internal flow force behind the exit rake was assumed negligible since no pressure forces existed over this portion of the duct (constant area section) and the skin-friction forces were assumed small.

A standard Wiancko pressure cell, used to measure the air-flow instability, was installed upstream of the compressor inlet (see fig. 1). The equipment necessary to operate the pressure cell consisted of a carrier oscillator driving an a-c bridge at 3000 cps. The alternating current resulting from an unbalance of the bridge was demodulated by a full wave crystal diode rectifier, and used to drive a Consolidated oscillograph with a 1000 cps galvanometer element. A grid of constant pressure lines spaced at even tenths of the tunnel stagnation pressure were superimposed on the oscillograph record so that values of the maximum total amplitude of the pressure pulsations occurring in the duct could be readily determined.

A four-component strain-gage balance mounted inside the model was used to measure the aerodynamic forces. The net drag, reduced to standard NACA form, was determined by subtracting the internal-flow force and base forces from the balance measured values.

The experimental data were obtained for Mach numbers of 0, 0.6, 0.9, 1.3, 1.5, 1.7, and 1.9 and, except for the static tests (M = 0), at a Reynolds number of 2.83 million. For the major portion of the tests data were obtained at the following angles of attack:

α	M
7.6°	0.6 and 0.9
4.1°	1.3
3.0°	1.5
0.85°	1.7 and 1.9

A complete angle-of-attack investigation ranging from 0° to 15° was made for the basic configuration, N_2L_2, and for two other configurations, $N_3L'_3$, and N_3L_2, throughout the Mach number range tested. Data were also obtained for the basic configuration between sideslip angles of $\pm 5^\circ$ at $\alpha = -0.3^\circ$. At each Mach number the mass-flow ratio was varied from near 0 to maximum obtainable by means of a movable plug at the model base.

The data were corrected for the following effects:

1. Induced effects of the tunnel walls at subsonic speeds resulting from lift on the model.

2. The longitudinal force on the model due to streamwise variation of the static pressure as measured in the empty test section.

3. The difference between the measured base pressure and the free-stream static pressure.

4. The angular deflection of the sting and balance under aerodynamic load.

5. The change in airspeed in the vicinity of the model at subsonic speeds resulting from the constriction of the flow by the tunnel walls.

The following table lists the estimated uncertainty introduced into each corrected nondimensional coefficient by the known uncertainties in the measurements:

Quantity	Uncertainty
C_D	± 0.0005
p_{t_c}/p_{t_∞}	± 0.005
m_c/m_∞	± 0.01
M_∞	± 0.03
R	$\pm 0.03 \times 10^6$
α	$\pm 0.15^\circ$

RESULTS

The pressure recovery for simulated take-off ($M_\infty = 0$) as a function of the air-flow parameter is presented in figure 7 for the three lip shapes under investigation. The pressure recoveries and drag coefficients as functions of mass-flow ratio for the different lip and nose shapes are included in figures 8 to 11. The effects of nose shape may be seen more clearly in figure 12 where the recovery and drag characteristics are shown as functions of Mach number at mass-flow ratios near typical inlet-engine matched conditions. The effects of angle of attack on pressure recovery and drag for configurations N_2L_2, $N_3L'_3$, and N_3L_2 are shown in figures 13, 14, 15, respectively. In figure 16 the effect of sideslip on pressure recovery is presented for the basic configuration, N_2L_2. Typical pressure-time records of the pressure cell mounted in the duct are illustrated in

figure 17. The mass-flow ratios where buzz occurred have been indicated in figures 8 through 16 by shaded symbols. Typical profile maps showing contour lines of constant pressure recovery around the compressor station for configurations N_3L_3 and N_3L_2 are presented in figure 18. The conditions that were selected correspond to mass-flow ratios near typical inlet-engine air-flow requirements at a Mach number of 1.5.

DISCUSSION

Pressure Recovery and Drag Characteristics

Effect of lip shape and diffuser shape.- For supersonic aircraft operating over a wide range of Mach numbers, the relative sharpness of the lip profile is of considerable importance. The lip shapes, similar to those of reference 4, were tested primarily to compare the differences in performance between the rounded and sharp lip shape for both subsonic and supersonic operation. For the take-off condition ($M_\infty = 0$, fig. 7) it can be seen that the blunt lips gave somewhat better performance. At supersonic speeds the results of this test show that the sharp lip (L_3) and the round lip (L_2) gave essentially the same pressure recoveries (see figs. 8(d), (e), and (f)). A comparison between the rounded lips (L_1 and L_2, fig. 9) showed that L_1 had slightly higher pressure recovery at $M_\infty = 1.5$, but lower pressure recovery at $M_\infty = 0.9$ due to a reduction of maximum mass-flow ratio. The lower values of maximum mass-flow ratio noted for L_1 may be attributed to the lip profile which resulted in a larger inlet area and a slightly smaller minimum throat area. The differences in drags between the three lip shapes were not large up to Mach numbers of 1.5 (see figs. 8(d) and 9). For Mach numbers of 1.7 and 1.9 the rounded lips seriously increased the drag of the model (figs. 8(e) and (f)). This increase in drag at the high supersonic Mach numbers may be attributed fundamentally to the increase in cowl wave drag of the blunt-lip configuration.

Examination of the duct cross-sectional area for lip 3 (fig. 5) revealed that the minimum internal cross-sectional area was well behind the lip entrance. Relieving the internal contraction (resulting in configuration L'_3) was expected to result in improvements in pressure recovery and mass-flow ratio. However, the data show that increased performance was not realized at all Mach numbers investigated. Measurable increases in the maximum mass-flow ratios occurred for Mach numbers from 0.9 to 1.9; however, a loss in pressure recovery occurred at reduced mass-flow ratios for Mach numbers of 1.7 and 1.9 (see fig. 8). As expected, this internal area alteration had negligible effects on the drag coefficient at the Mach numbers tested.

Effect of nose shape.- Although the nose shapes tested did not involve a systematic variation of isolated geometric variables, they did afford

deviations in nose lengths (or fineness ratio) compression surface angle, and nose roundness. Comparison of the five nose shapes at typical inlet-engine matched mass-flow ratios (fig. 12) shows that the configurations with the shortest pointed nose (N_4) gave the highest pressure recovery at supersonic speeds. The nose shape showing the lowest drag over the supersonic speed range was seen to be the long rounded nose, N_2. At the subsonic Mach number, $M_\infty = 0.9$, the nose shapes had only small effects on pressure recovery and drag near maximum mass-flow ratios (figs. 10(a) and 11(a)).

The effect of nose rounding on the performance characteristics can be illustrated by comparing, near maximum mass-flow ratios, the two long nose shapes, N_1 (pointed) and N_2 (rounded), and the two short nose shapes, N_4 (pointed) and N_5 (rounded). The data showed (fig. 12(a)) that the rounded nose configurations resulted in lower drag coefficients at supersonic speeds than the corresponding pointed nose configurations. As would be expected the short nose shapes had larger drag than the longer nose shapes. However, blunting the long nose shapes slightly increased the recovery; whereas blunting the short nose shapes appreciably decreased the pressure recovery.

Examination of the data in figure 12 shows that, generally, the pressure-recovery losses became greater and the drag decreased as the slope of the nose surfaces decreased (compare nose shapes 4, 3, and 2, respectively). The decrease in pressure recovery can be attributed to increased pressure losses through the oblique and normal-shock-wave combinations associated with each nose shape, while the decrease in drag is the result of the decrease in the effective angle of the nose surfaces.

Though these two-shock inlet configurations, generally, had better than normal shock recovery, it is felt that further improvements are possible at the high supersonic Mach numbers with this type of inlet. For example, observation of schlieren pictures showed that the oblique shock was well ahead of the cowl lip at $M_\infty = 1.9$. However, in reference 5, the best combination of pressure recovery and drag occurred when the oblique shock fell just upstream of the cowl lip ($M_\infty = 2.0$). It would be expected therefore, that a forward movement of the cowl lip might improve the drag characteristics of the inlet configurations. Also, in moving the cowl lip forward the normal shock would be shifted upstream on the nose surfaces to a position ahead of the expansion region on the nose and, therefore, to a region of lower local Mach number.

During this investigation it was seen that the forenose boundary-layer air was entering the inlet. The results of references 1 and 6 have shown that boundary-layer air could be efficiently diverted around a circular inlet. It is believed, then, that a circular inlet with a boundary-layer diverter (see ref. 1) would improve the performance characteristics for this air-induction system over the entire Mach number range of this test.

Effect of angle of attack.- Three configurations were investigated (N_2L_2, $N_3L'_3$ and N_3L_2) to illustrate the effect of angle of attack on pressure recovery and drag coefficient. It is shown in figures 13, 14, and 15 that large increases in angle of attack indicated no unfavorable effects on the pressure recovery over the normal engine operating mass-flow ratios. At Mach numbers from 0.6 to 1.3, the pressure-recovery results shown for configurations N_2L_2 and $N_3L'_3$ were essentially independent of angle of attack up to approximately 15°. The increase in supersonic compression as a result of increasing the angle of attack of the basic configuration N_2L_2 to 7° led to considerable increases in pressure recovery at Mach numbers above 1.3. Consequently, the surface of nose 2 was redesigned to take effective advantage of the supersonic compression at low angles of attack (see fig. 4, nose 3). The data for configurations $N_3L'_3$ and N_3L_2 (figs. 14 and 15) showed that the pressure recovery was nearly independent of angle of attack up to $M_\infty = 1.5$, and that the favorable pressure recovery attained for configuration N_2L_2 at $\alpha = 7°$ was obtained at the lower angles of attack of 0° and 3.0°. At Mach numbers above 1.5 the pressure recovery was no longer independent of angle of attack, though the values of pressure recovery obtained for configurations $N_3L'_3$ and N_3L_2 at each angle of attack were higher than that obtained for configuration N_2L_2.

The change in drag coefficient with increasing angle of attack up to approximately 4° was not large; however, further increases in angle of attack resulted in substantial drag penalties for all configurations.

Air-Flow Stability

The criterion used to indicate the degree of instability of the inlets investigated was the maximum total amplitude of the pressure oscillations that were recorded on the oscillograph. It appeared from the pressure-time records (see fig. 17) that the pressure oscillations were random, and, as pointed out in reference 7, that the static-pressure fluctuations were caused by the separated flow associated with boundary-layer shock-wave interaction. From a study of the buzz records, it was found that only small static-pressure fluctuations were recorded for the various configurations tested (no buzz data obtained for $N_3L'_3$) at Mach numbers of 1.5 and below. At Mach numbers of 1.7 and 1.9, flow instability generally occurred at mass-flow ratios below about 0.7. The effect of configuration changes on air-flow stability was small throughout the Mach number range investigated.

A possible explanation for negligible flow instability at the high mass-flow ratios, particularly at $M_\infty = 1.9$, may be that though the pressure rise across the normal shock induced separation ahead of the inlet, the slope of the nose surface and a favorable pressure gradient behind the normal shock caused reattachment of the separated flow. It was shown in

reference 8 that reducing the diffusion rate to zero (no internal cross-sectional area change for approximately 3.5 lengths of hydraulic diameters) immediately behind the inlet reduced the mass-flow range for flow pulsation at Mach numbers of 1.8 and 2.0. Though the relation between the mechanism inciting flow instability and the inlet geometry parameters is not fully understood, it appears that favorable pressure gradients ahead of the inlet and a short distance inside the inlet lead to a wider range of stable mass-flow ratios.

In figure 17, typical buzz records show the static-pressure fluctuations that occurred at $M_\infty = 1.9$ for configuration N_3L_3. Flight operation below mass-flow ratios where flow instability was first noted at Mach numbers of 1.7 and 1.9 would appear to be hazardous since the pressure pulsations were observed to develop rapidly once buzz started.

Compressor Face Total-Pressure Distribution

In air-inlet systems where the internal air passage of the duct is curved and has an asymmetrical cross section, the pressure gradients at the engine station may be large enough not only to effect seriously the net thrust and acceleration characteristics of an engine operating at high speeds, but to cause large vibratory stresses in the compressor blades. A typical total-pressure map, shown in figure 18, indicates no circumferential or radial distortions greater than 7 percent of the total pressure near the "matched" mass-flow ratio for the inlet supplying air to a typical jet engine at a Mach number of 1.5. The effect of lip shape (L_2 or L_3) showed no pronounced differences in local pressures at the compressor station. Observations of the pressure maps for the other nose- and lip-shape combinations (data not shown) for angles of attack up to 7° at $M_\infty = 1.5$ and for Mach numbers of 1.7 and 1.9 at $\alpha = 0.85^\circ$ indicated no greater radial or circumferential gradients than those shown in figure 18.

Propulsive-Thrust Analysis

Since neither pressure recovery nor drag can provide the proper criterion for comparative evaluation of the configurations tested, a significant performance comparison involving a conversion of the drag force and pressure recovery into a single propulsive thrust parameter ($\eta = (T_N - D)/T_{isen}$) has been utilized. In this analysis the engine and inlet were compared at their actual operating condition where the air supplied by the inlet must equal the air required by the engine. The thrusts were derived from the J-57 engine data operating at 35,000 feet. (Analyses made for other altitudes did not alter the general shape of the curves presented in fig. 19.) Further detailed information regarding the method and assumptions involved in this performance analysis are given in reference 4.

The results of the analysis for only the five best configurations tested are given in figure 19. The results for configuration $N_3L'_3$ were omitted because the parameter η for configuration N_3L_3 was equal or slightly superior at the Mach numbers investigated. Configuration N_3L_3 can be seen to have considerably better propulsive efficiency than the other inlets tested at supersonic speeds. At subsonic speeds (M_∞ = 0.6 and 0.9), little difference between configurations N_3L_3 and N_2L_2 were noted. A significant fact gained from figure 20 was the superiority of the sharp-lip inlet over the rounded-lip inlet (L_3 and L_2, respectively) at Mach numbers above 1.5. The difference in η between the sharp and rounded lips represents approximately 1000 pounds in available airplane thrust at a Mach number of 1.9 (assuming an altitude of 35,000 feet). This marked gain, however, diminishes to approximately 350 pounds of available thrust at M_∞ = 1.5. Also, it was observed from the analysis that nose 3 was the superior nose shape at Mach numbers above 1.5 and, in combination with lip 3 for the design inlet area, was superior at Mach numbers of 1.5 and 0.9.

The design inlet area simulated in the tests (4.07 square feet for L_2 and L_3) appeared to be a good compromise when the performance in the speed range from 0 to 1.5 was considered. Above Mach numbers of 1.5, however, a variable-area inlet or an internal bypass system would be necessary if optimum operation were to be obtained.

CONCLUSIONS

An air-induction system for a proposed high-speed fighter airplane has been investigated at Mach numbers from 0 to 1.9. The results of this investigation indicated the following:

1. The underslung nose type of air-induction system has the inherent advantage of being able to operate over a large positive angle-of-attack range with no deleterious effects on pressure recovery.

2. Of the inlets investigated, none was markedly superior over the entire range of operating variables, though in the supersonic speed range that configuration having the long rounded nose, designed to increase the supersonic compression at low angles of attack, and a sharp lip (configuration N_3L_3) had the highest propulsive thrust.

3. From consideration of over-all performance of the different lip shapes, the use of a rounded lip would give satisfactory performance up to M_∞ = 1.5. However, at Mach numbers above 1.5 the rounded lips investigated seriously increased the drag.

4. The analysis showed that a fixed inlet area could be used without seriously affecting the performance of an airplane for Mach numbers up to

[redacted]

1.5; however, if optimum performance were desired at higher Mach numbers, a variable-area inlet or a bypass system would be required for this air-induction model.

5. A study of the air-flow stability revealed no serious flow oscillations throughout the Mach number range investigated for normal engine operation.

6. Compressor total-pressure distributions showed no circumferential or radial distortions greater than 7 percent of the total pressure near the engine "matched" mass-flow ratio at the Mach numbers tested.

Ames Aeronautical Laboratory
National Advisory Committee for Aeronautics
Moffett Field, Calif., July 13, 1955

REFERENCES

1. Merlet, Charles F., and Carter, Howard S.: Total Pressure Recovery of a Circular Underslung Inlet With Three Different Nose Shapes at a Mach Number of 1.42. NACA RM L51K05, 1952.

2. Merlet, Charles F.: Pressure Recovery and Drag Characteristics of a Forward Located Circular Scoop Inlet as Determined From Flight Tests From Mach Numbers From 0.8 to 1.6. NACA RM L54B23, 1954.

3. Frick, Charles W., and Olson, Robert N.: Flow Studies in the Asymmetric Adjustable Nozzle of the Ames 6- by 6-Foot Supersonic Wind Tunnel. NACA RM A9E24, 1949.

4. Mossman, Emmet A., and Anderson, Warren E.: The Effect of Lip Shape on a Nose-Inlet Installation at Mach Numbers From 0 to 1.5 and a Method for Optimizing Engine-Inlet Combinations. NACA RM A54B08, 1953.

5. Gorton, Gerald C.: Investigation at Supersonic Speeds of a Translating-Spike Inlet Employing a Steep-Lip Cowl. NACA RM E54G29, 1954.

6. Mossman, Emmet A., Pfyl, Frank A., and Lazzeroni, Frank A.: Experimental Investigation at Mach Numbers from 0 to 1.9 of Trapezoidal and Circular Side Inlets for a Fighter-Type Airplane. NACA RM A55D27, 1955.

7. Mossman, Emmet A., Lazzeroni, Frank A., and Pfyl, Frank A.: An Experimental Investigation of the Air-Flow Stability of a Scoop-Type Normal Shock Inlet. NACA RM A55A13, 1955.

8. Nettles, J. C.: The Effect of Initial Rate of Subsonic Diffusion on The Stable Subcritical Mass-Flow Range of a Conical Shock Diffuser. NACA RM E53E26, 1953.

TABLE I.- NOSE COORDINATES
[Dimensions in inches]

Inlet Entrance

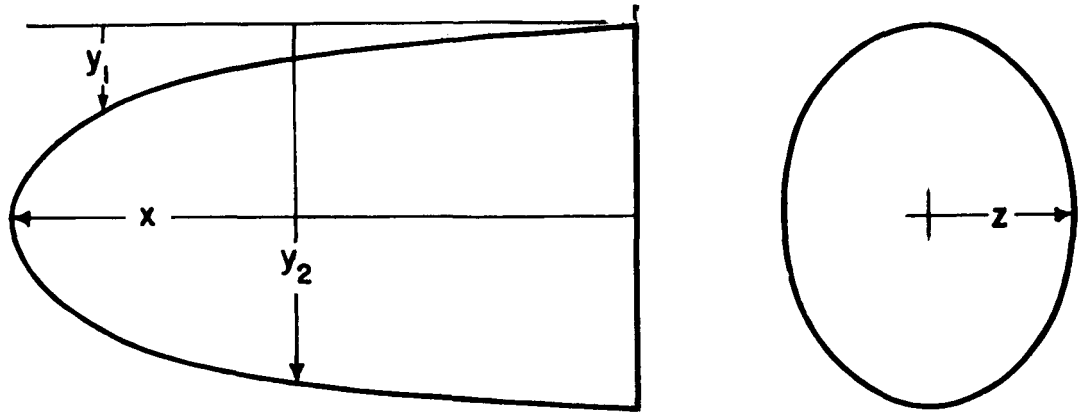

Nose 1				Nose 2				Nose 3			
No L.E.R.				L.E.R.=0.13 (side view) L.E.R.=0.07 (top view)				L.E.R.=0.09 (side view) L.E.R.=0.11 (top view)			
x	y_1	y_2	z	x	y_1	y_2	z	x	y_1	y_2	z
0	0	2.25	1.04	0	0	2.25	1.04	0	0	2.25	1.04
.40	.12	2.21	.93	.40	.11	2.19	.95	.40	.11	2.17	.95
.80	.25	2.12	.84	.80	.24	2.11	.86	.80	.24	2.06	.86
1.20	.41	2.02	.74	1.20	.38	2.00	.74	1.20	.38	1.93	.74
1.70	.62	1.85	.57	1.60	.55	1.89	.62	1.60	.55	1.79	.62
2.00	(1)	(1)	(1)	2.00	.73	1.77	.47	2.00	.73	1.61	.47
2.40	↓	↓	↓	2.40	.92	1.62	.33	2.40	.92	1.43	.29
2.80				2.91	1.31	1.31	0	2.73	1.19	1.19	0
3.10	1.26	1.26	0								

Nose 4				Nose 5			
No L.E.R.				L.E.R.=0.25 (side view) L.E.R.=0.12 (top view)			
x	y_1	y_2	z	x	y_1	y_2	z
0	0	2.25	1.04	0	0	2.25	1.04
.29	.11	2.17	.95	.40	.11	2.19	.95
.58	.24	2.08	.85	.80	.24	2.11	.86
.90	.40	1.94	.72	1.20	.38	2.00	.74
1.50	(1)	(1)	(1)	1.60	.55	1.87	.62
2.00	↓	↓	↓	2.00	.78	1.69	.43
2.61	1.26	1.26	0	2.40	1.26	1.26	0

[1]Straight line.

TABLE II.- LIP COORDINATES
[Dimensions in inches]

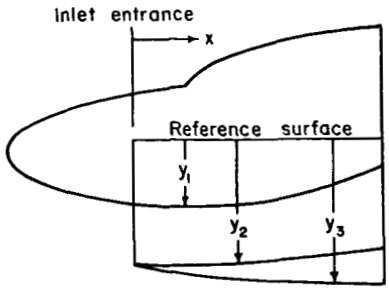

Lip 1				Lip 2				Lip 3			
L.E.R. = 0.025				L.E.R. = 0.020				L.E.R. = 0.004			
x	y_1	y_2	y_3	x	y_1	y_2	y_3	x	y_1	y_2	y_3
0	1.424	2.635	2.635	0	1.424	2.531	2.531	0	1.424	2.531	2.531
.05	1.435	2.585	2.670	.05	1.435	2.491	2.584	.05	1.435	2.526	2.541
.10	1.441	2.570	2.689	.10	1.441	2.486	2.618	.10	1.441	↓	2.548
.15	1.452	2.560	2.703	.15	1.452	2.486	2.639	.15	1.452	↓	2.555
.20	1.460	2.551	2.714	.20	1.460	2.489	2.659	.20	1.460	↓	2.561
.30	1.473	2.541	2.733	.30	1.473	2.495	2.690	.30	1.473	↓	2.575
.50	1.492	2.527	2.767	.50	1.492	2.506	2.738	.50	1.492	↓	2.601
.75	1.506	2.526	2.800	.75	1.506	2.517	2.785	.75	1.506	↓	2.636
1.00	1.513	↓	2.830	1.00	1.513	2.522	2.823	1.00	1.513	↓	2.669
1.30	1.511	↓	2.862	1.30	1.511	2.526	2.862	1.30	1.511	↓	2.709
1.60	1.502	↓	2.896	1.60	1.502	2.526	2.896	1.60	1.502	↓	2.749
2.00	1.483	2.522	2.929	2.00	1.483	2.522	2.929	2.00	1.483	2.522	2.802
2.40	1.463	2.501	2.951	2.40	1.463	2.501	2.951	2.40	1.463	2.501	2.857
2.80	1.441	2.473	2.967	2.80	1.441	2.473	2.967	2.80	1.441	2.473	2.910
3.20	1.428	2.456	2.977	3.20	1.428	2.456	2.977	3.20	1.428	2.456	2.957
3.60	1.396	2.445	2.985	3.60	1.396	2.445	2.985	3.60	1.396	2.445	2.981
4.03	1.361	2.440	2.989	4.03	1.361	2.440	2.989	4.03	1.361	2.440	2.989

Lip'3				Lip'3			
L.E.R. = 0.004				L.E.R. = 0.004			
x	y_1	y_2	y_3	x	y_1	y_2	y_3
0	1.424	2.531	2.531	1.30	1.405	↓	2.709
.05	1.435	2.526	2.541	1.60	1.382	↓	2.749
.10	1.440	↓	2.548	2.00	1.352	2.522	2.802
.15	1.449	↓	2.555	2.40	1.323	2.501	2.857
.20	1.454	↓	2.561	2.80	1.292	2.473	2.910
.30	1.462	↓	2.575	3.20	1.263	2.456	2.957
.50	1.461	↓	2.601	3.60	1.234	2.445	2.981
.75	1.446	↓	2.636	4.03	1.200	2.440	2.989
1.00	1.428	↓	2.669				

[redacted]

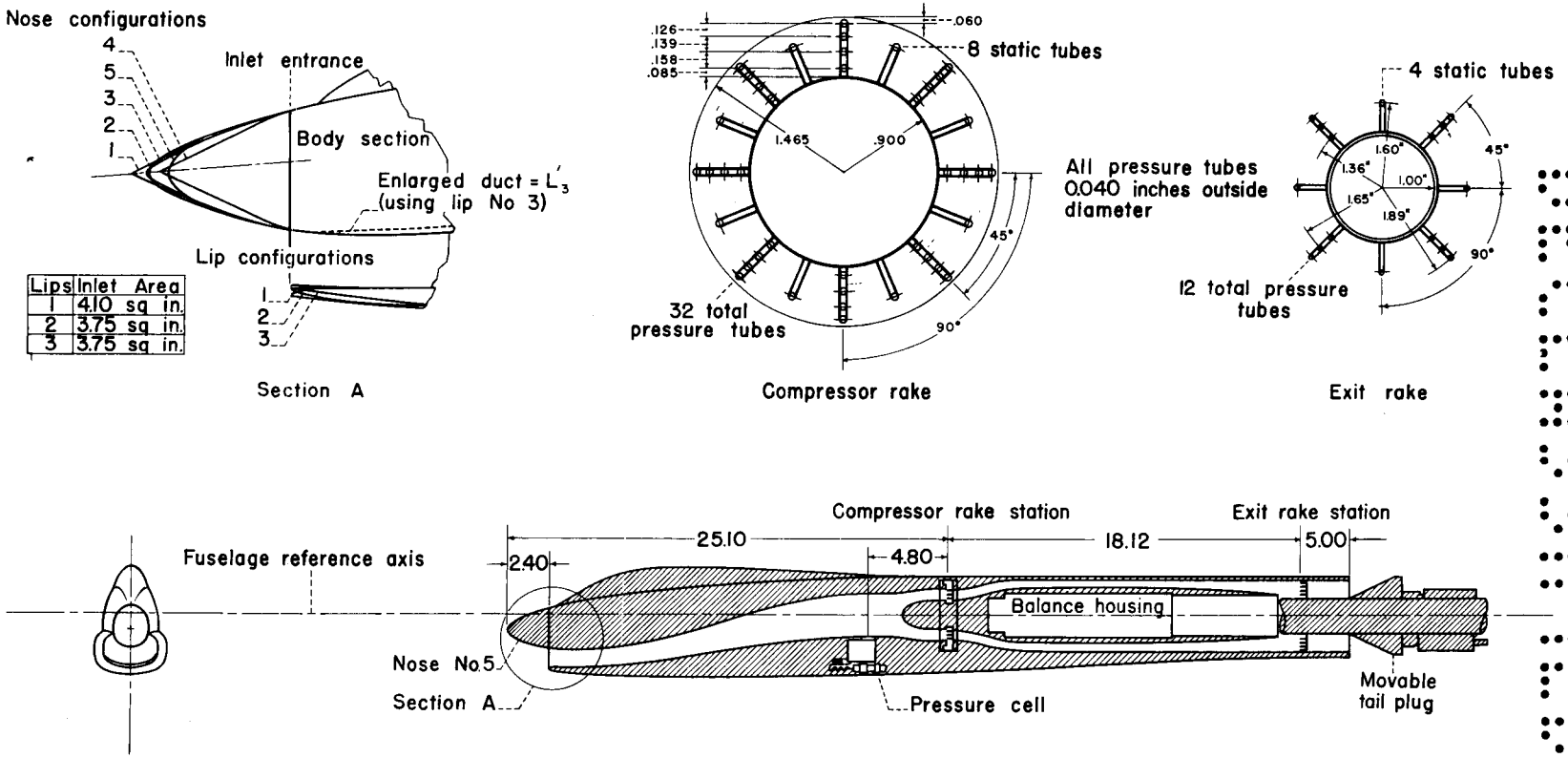

Figure 1.- Sketch of the air-induction model.

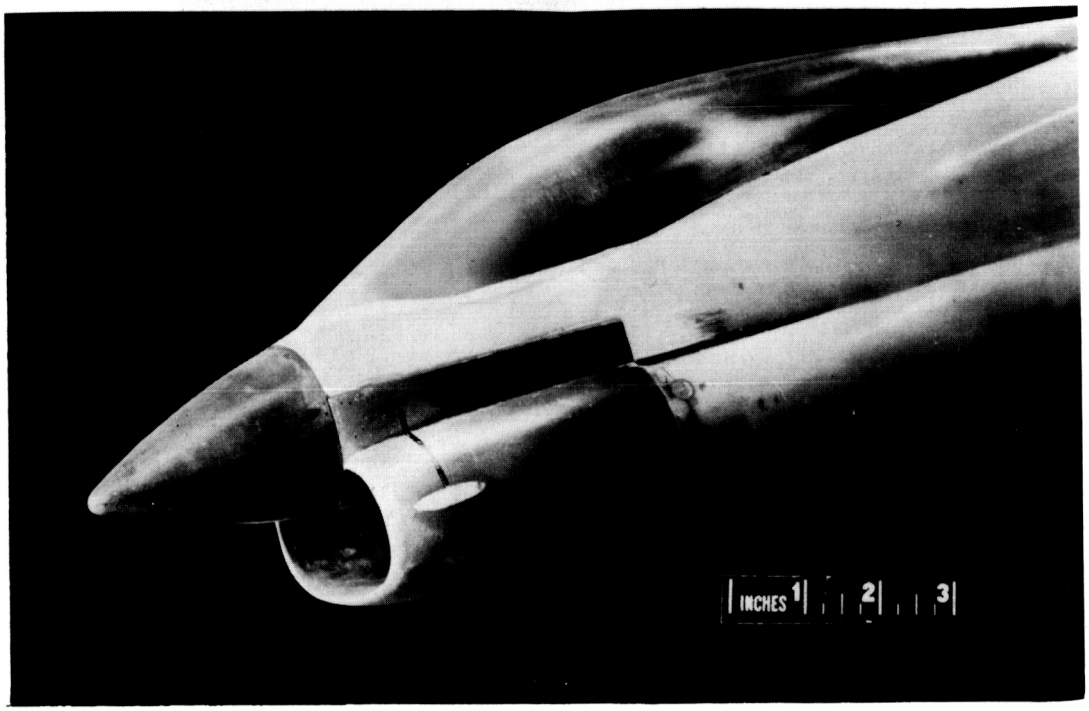

A-19851

(a) N_2L_2

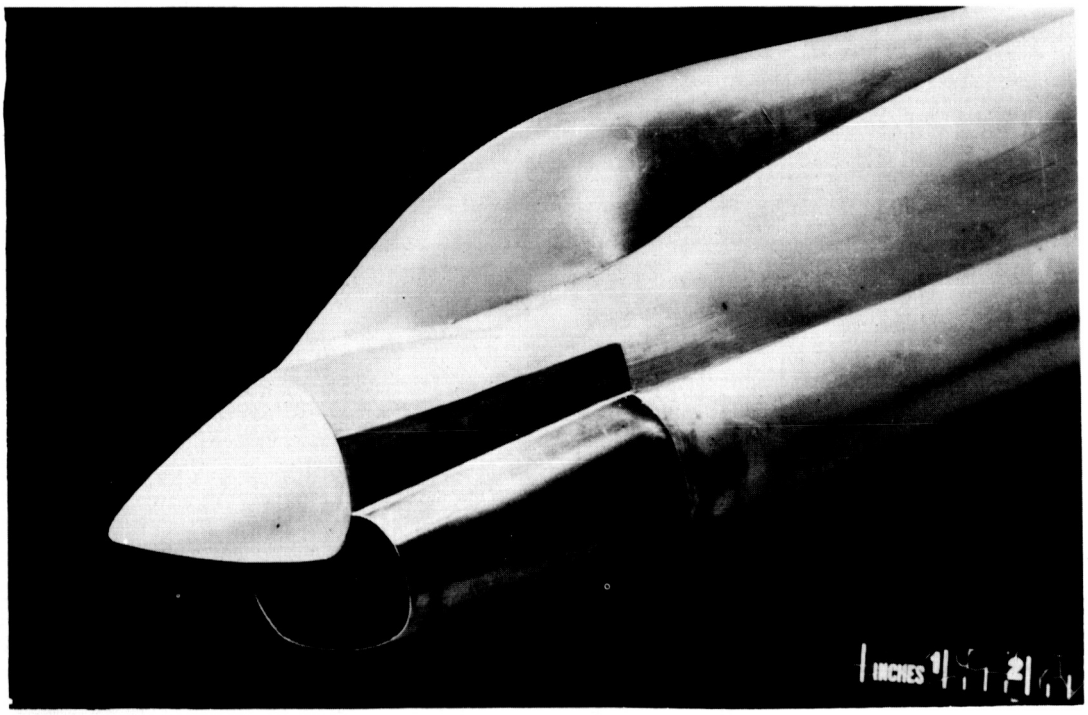

A-19850

(b) N_3L_3

Figure 2.- Photographs of the different nose and lip shapes.

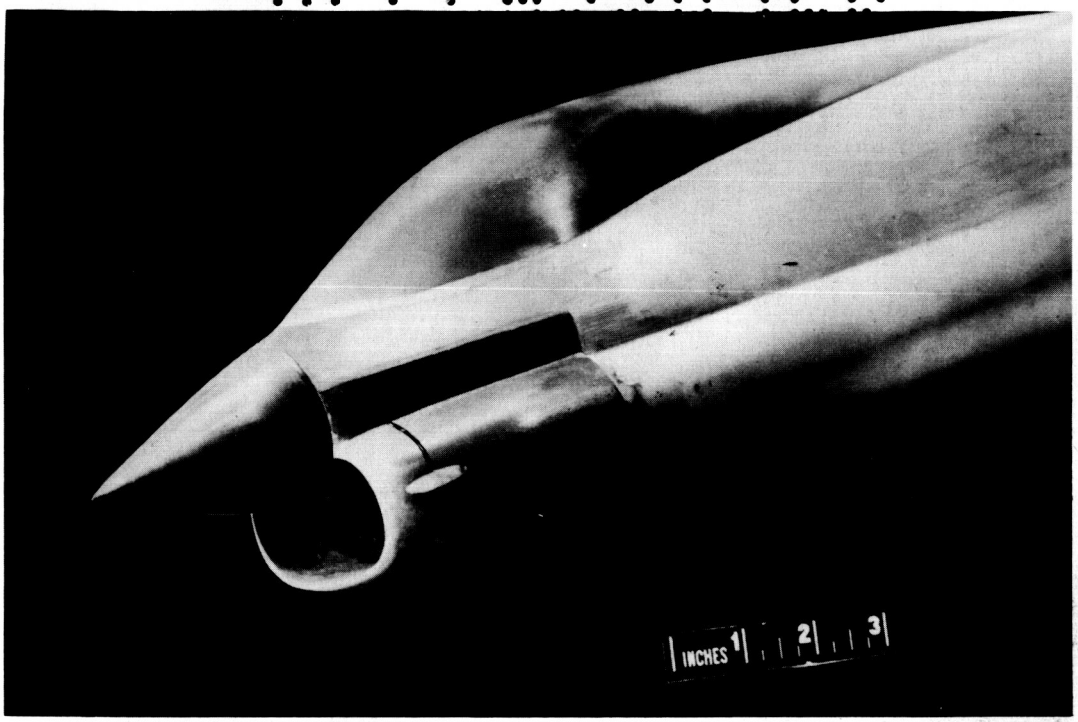

A-19848

(c) N_1L_2

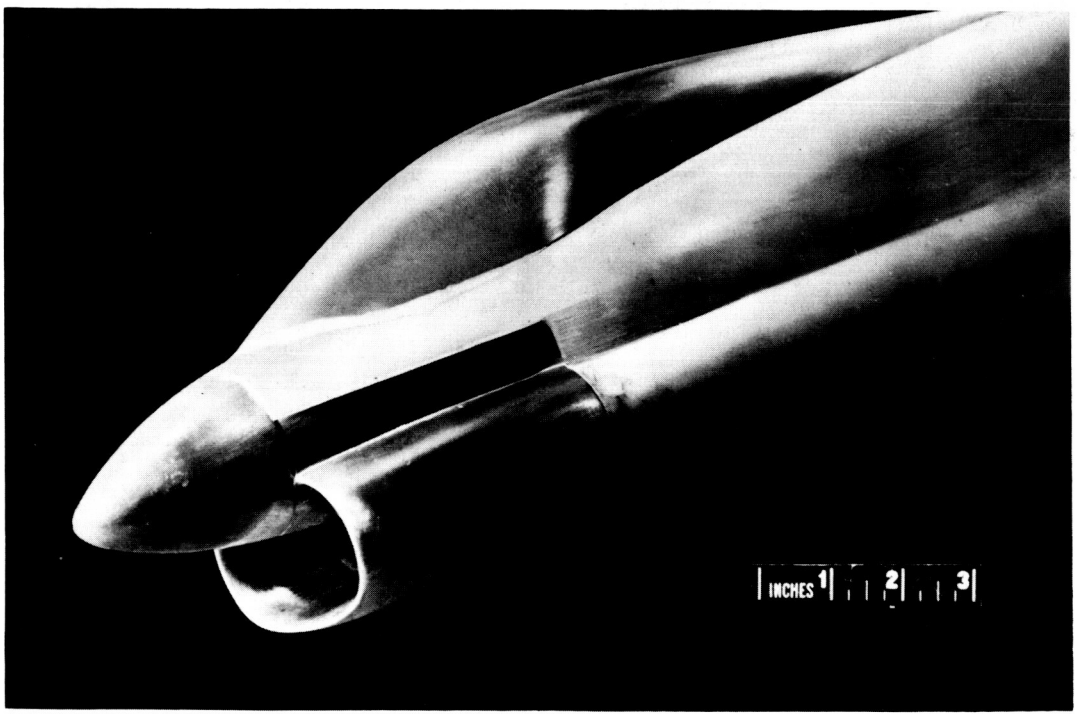

A-19849

(d) N_5L_1

Figure 2.- Continued.

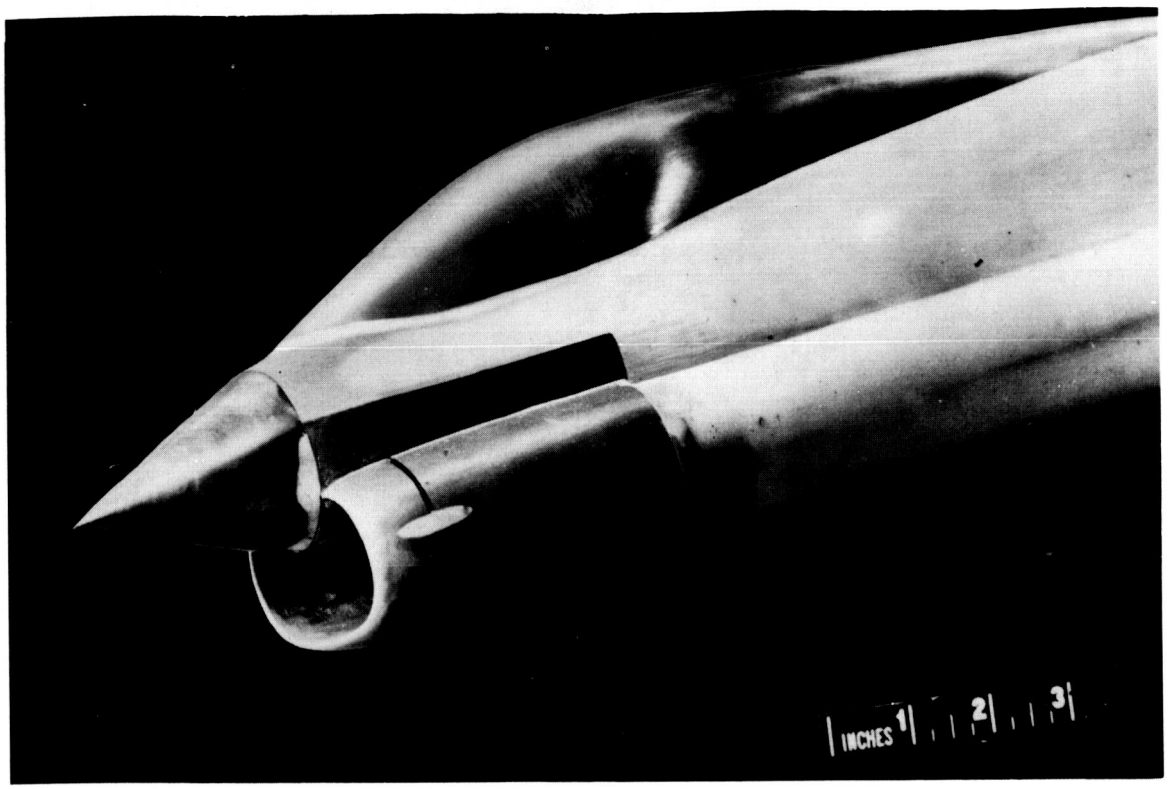

A-19852

(e) N_4L_2

Figure 2.- Concluded.

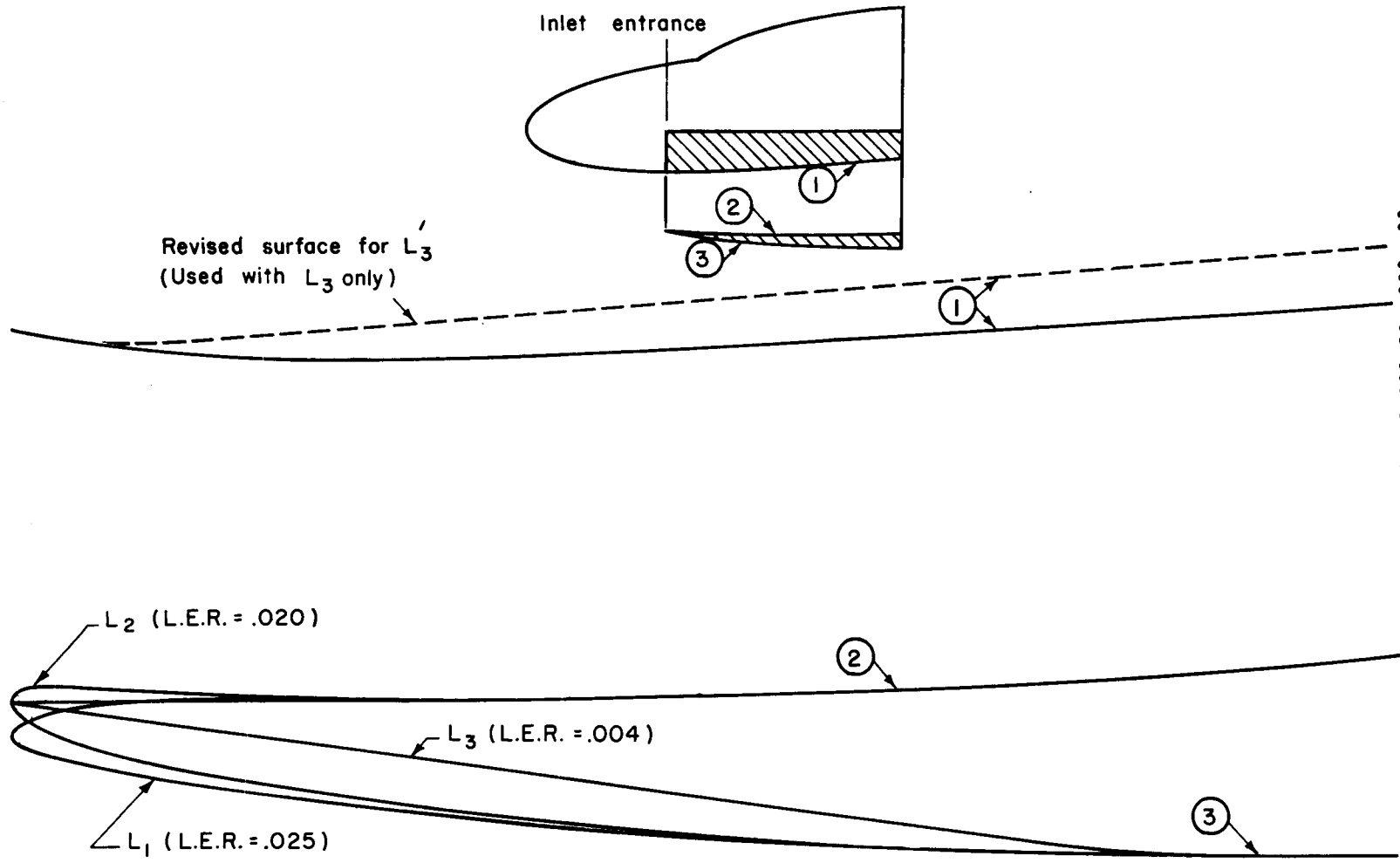

Figure 3.- Sketch showing the various lip configurations.

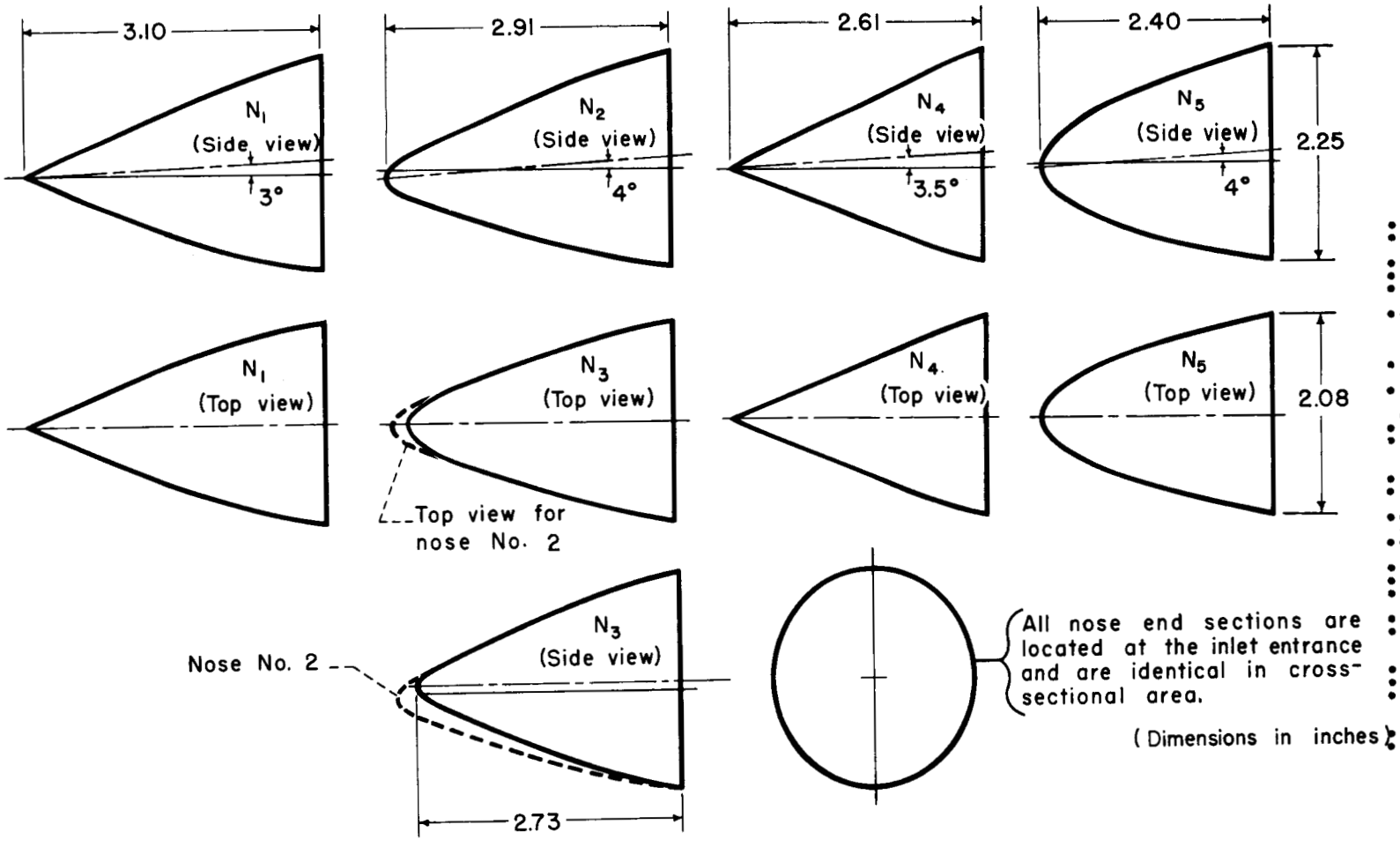

Nose configurations

Figure 4.- Sketch showing the various nose configurations.

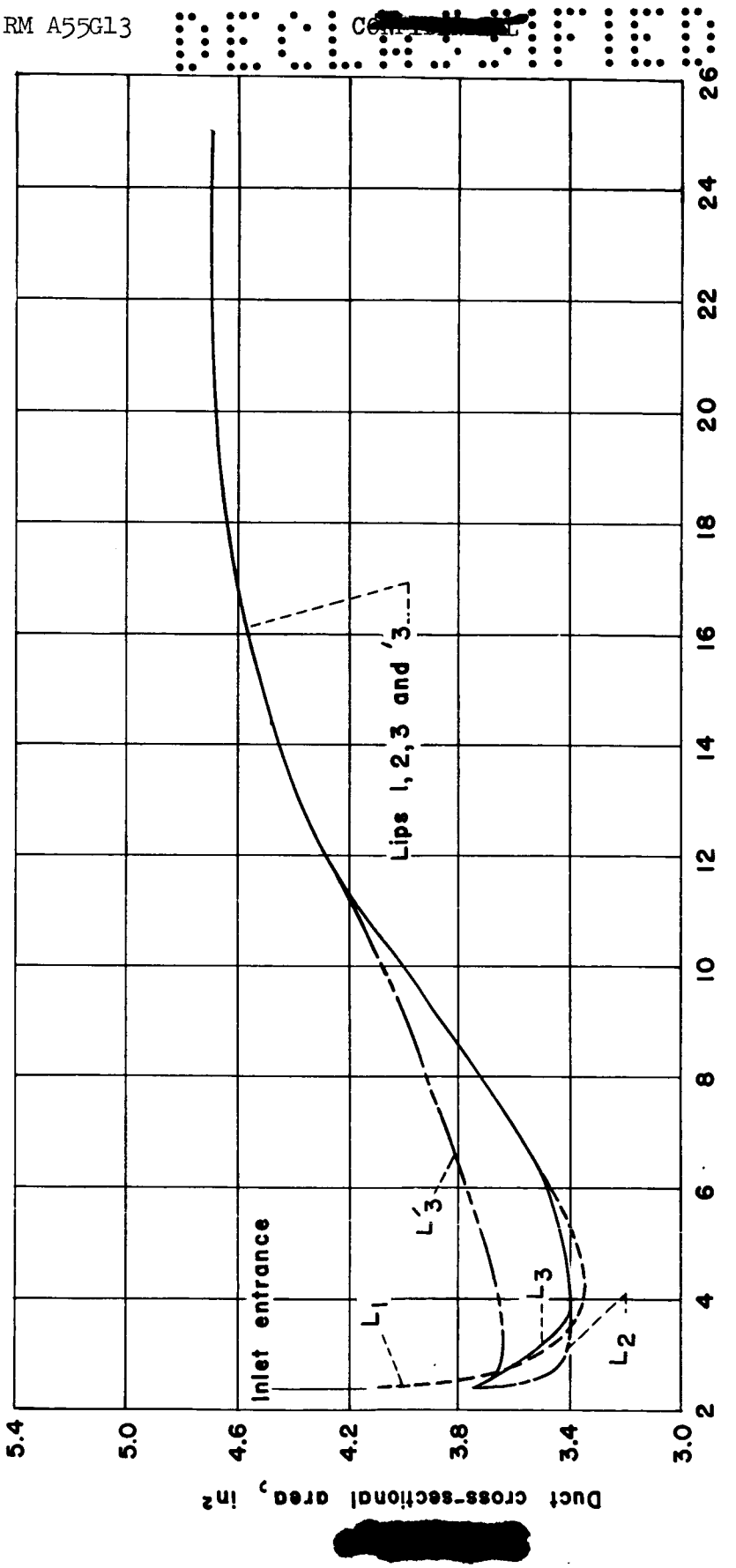

Figure 5.- Area distribution of diffuser for the various inlet configurations.

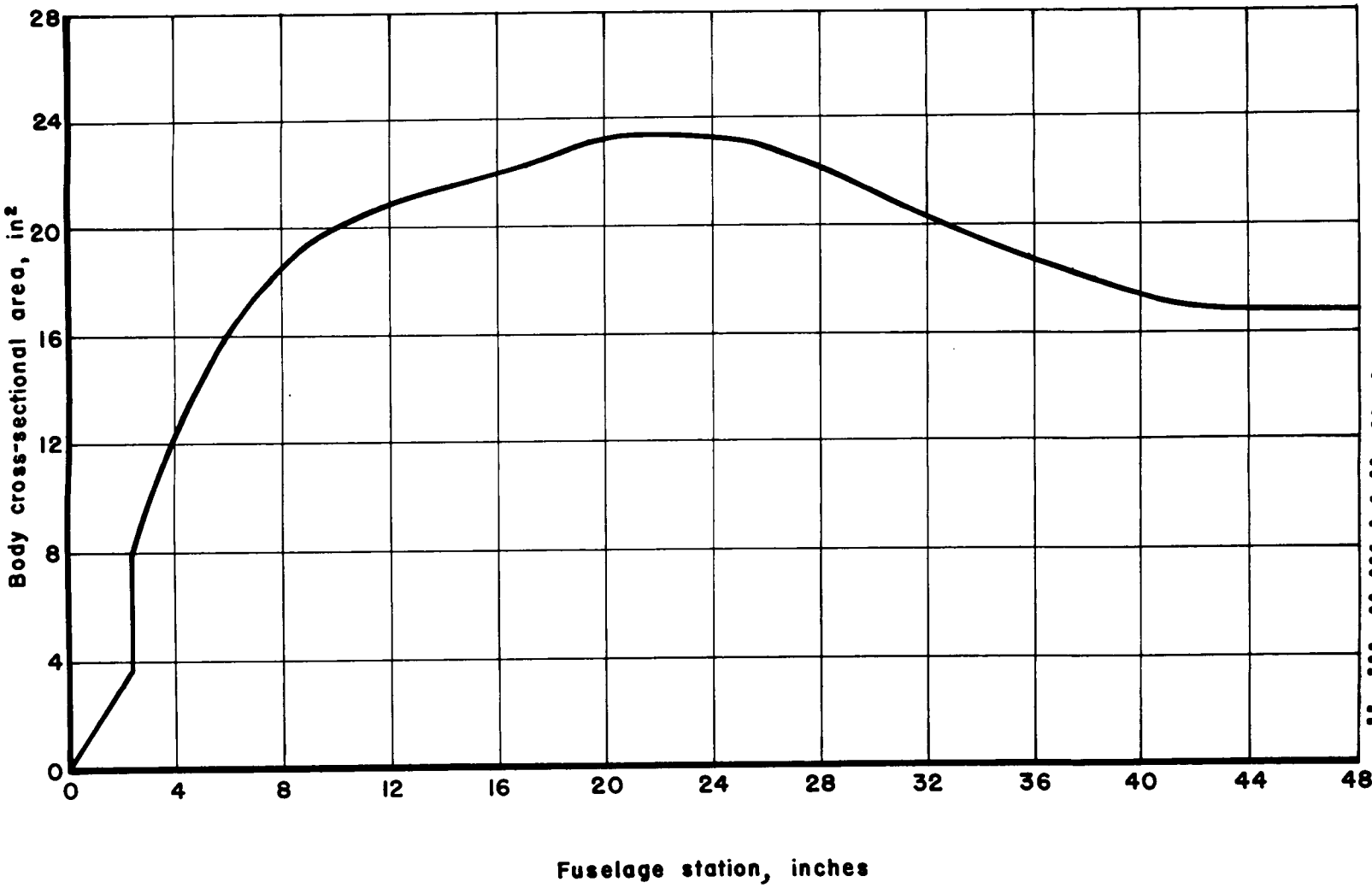

Figure 6.- Body cross-sectional area distribution of the model.

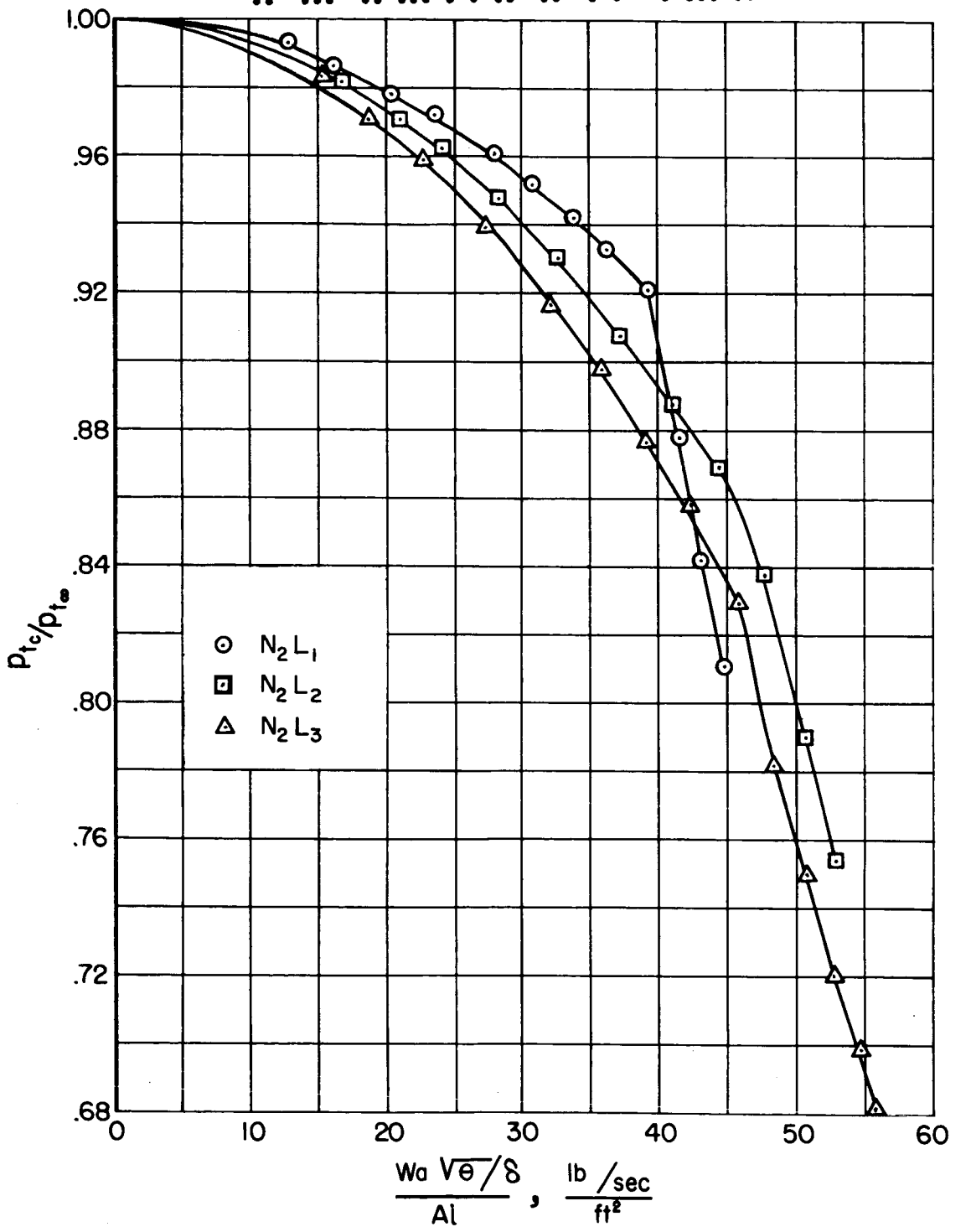

Figure 7.- The variation of pressure recovery with air-flow parameter for the take-off condition ($M_\infty = 0$).

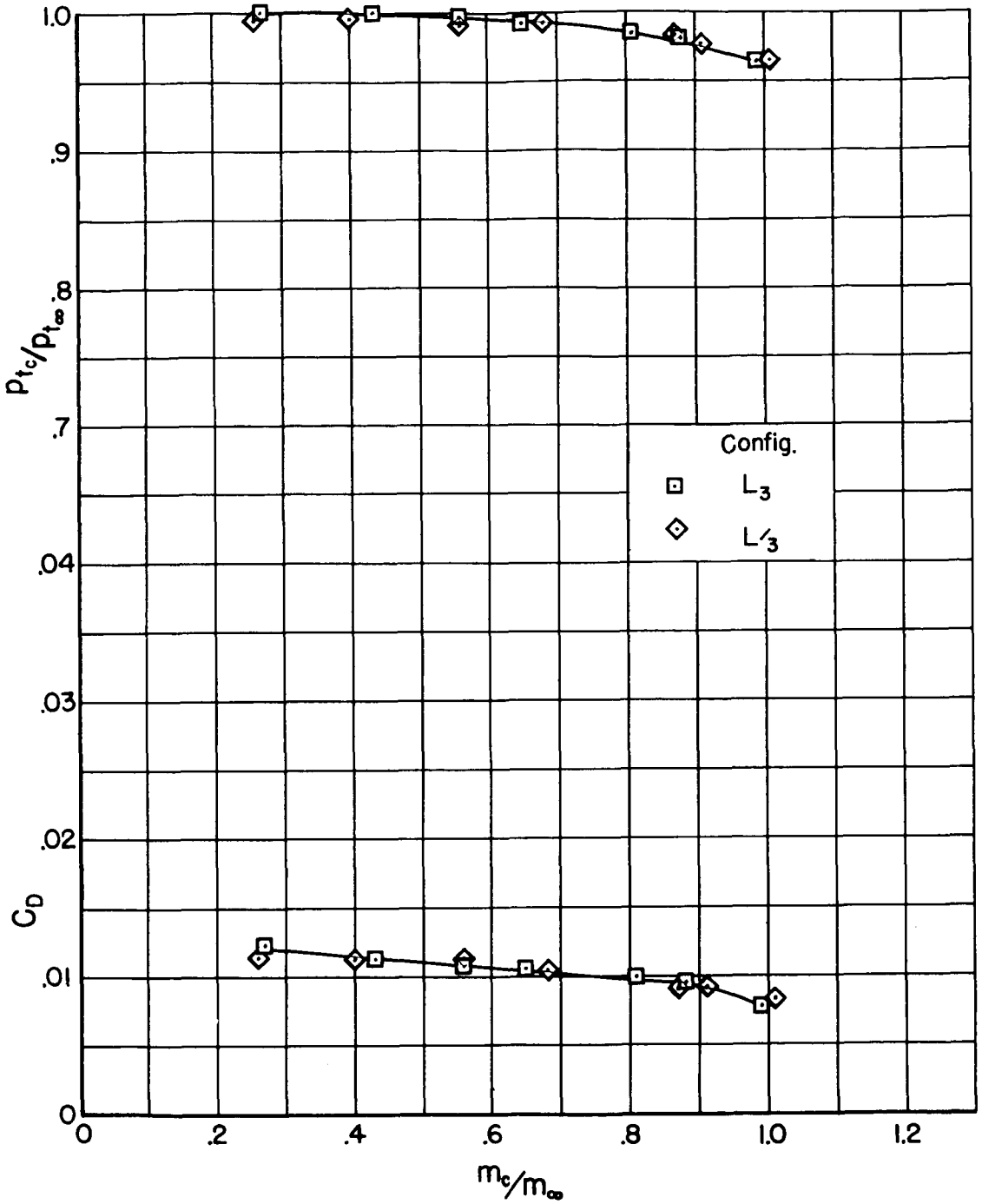

(a) $M_\infty = 0.6$; $\alpha = 7.6^\circ$

Figure 8.- Effect of changes in lip shape and diffuser cross-sectional area on the pressure recovery and drag with nose number 3.

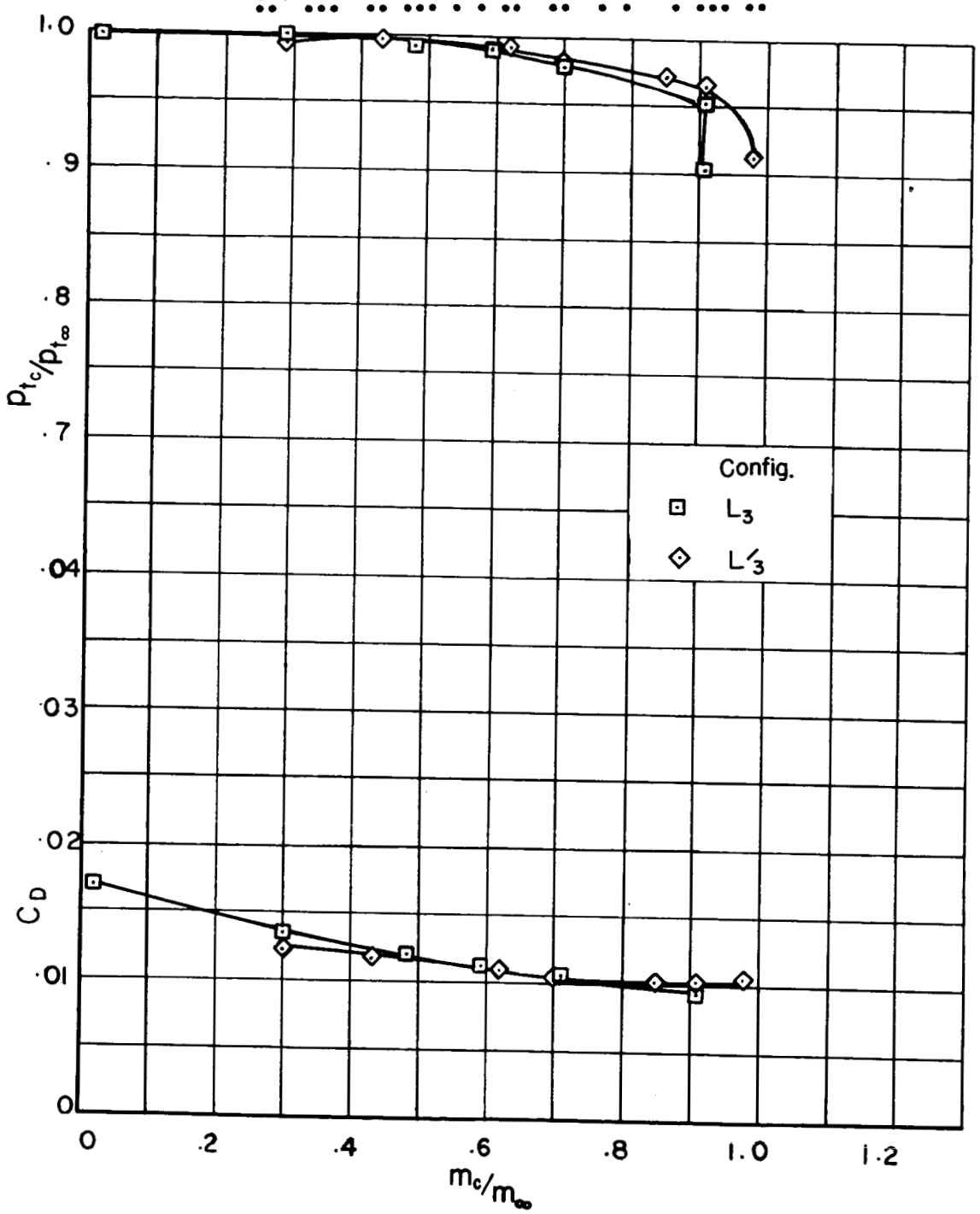

(b) $M_\infty = 0.9$; $\alpha = 7.6^\circ$

Figure 8.- Continued.

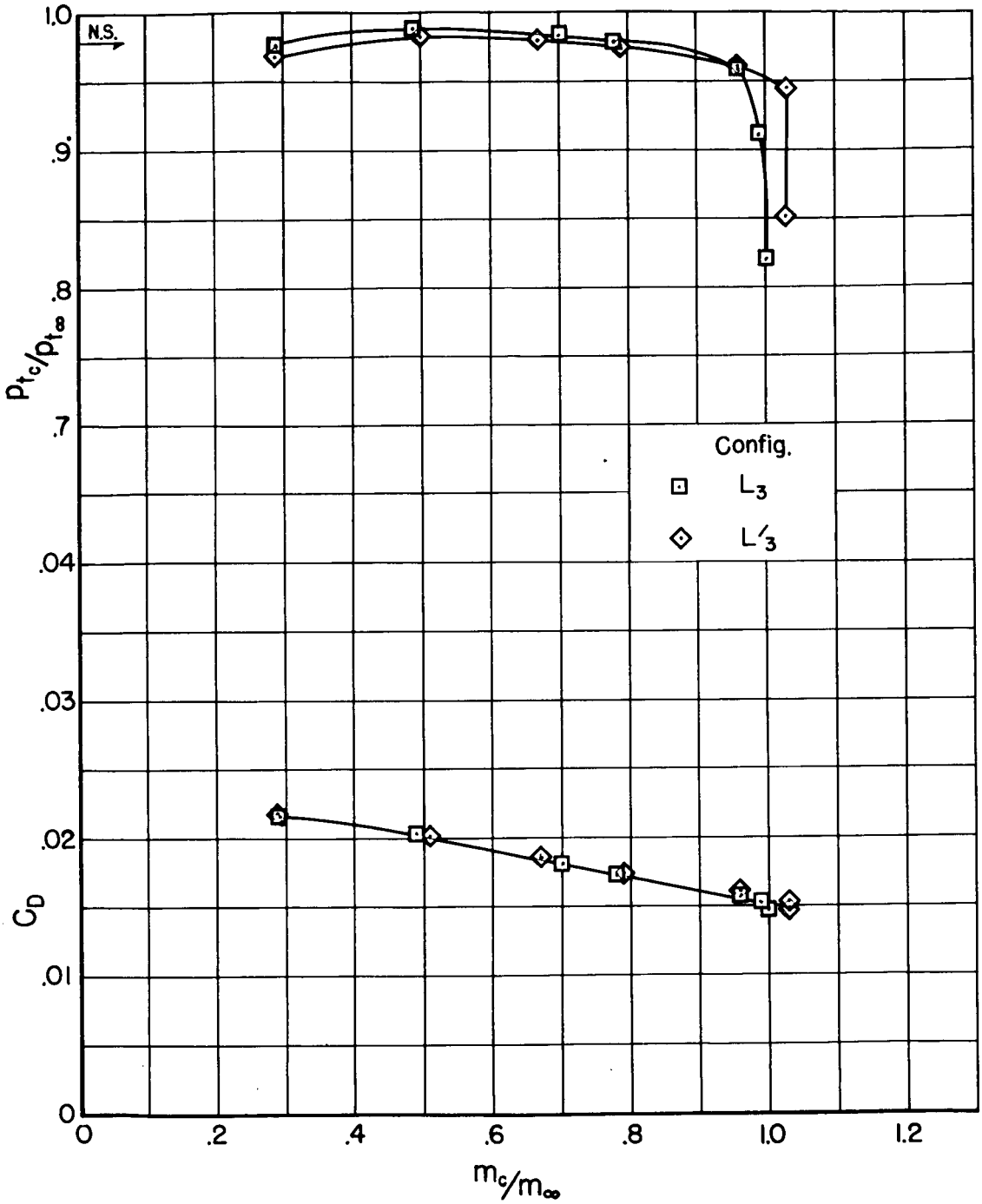

(c) $M_\infty = 1.3$; $\alpha = 4.1^\circ$

Figure 8.- Continued.

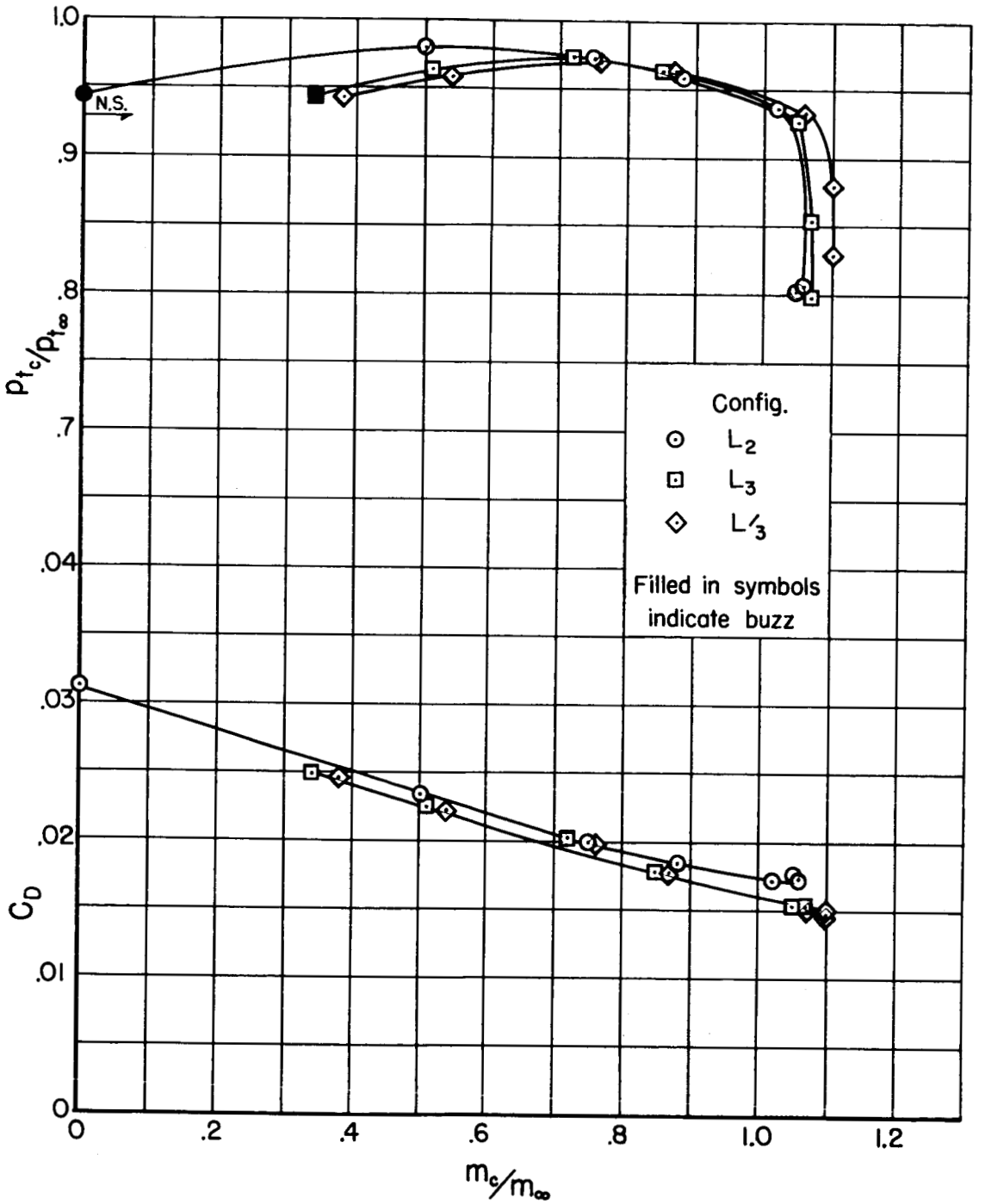

(d) $M_\infty = 1.5$; $\alpha = 3.0^\circ$

Figure 8.- Continued.

[redacted]

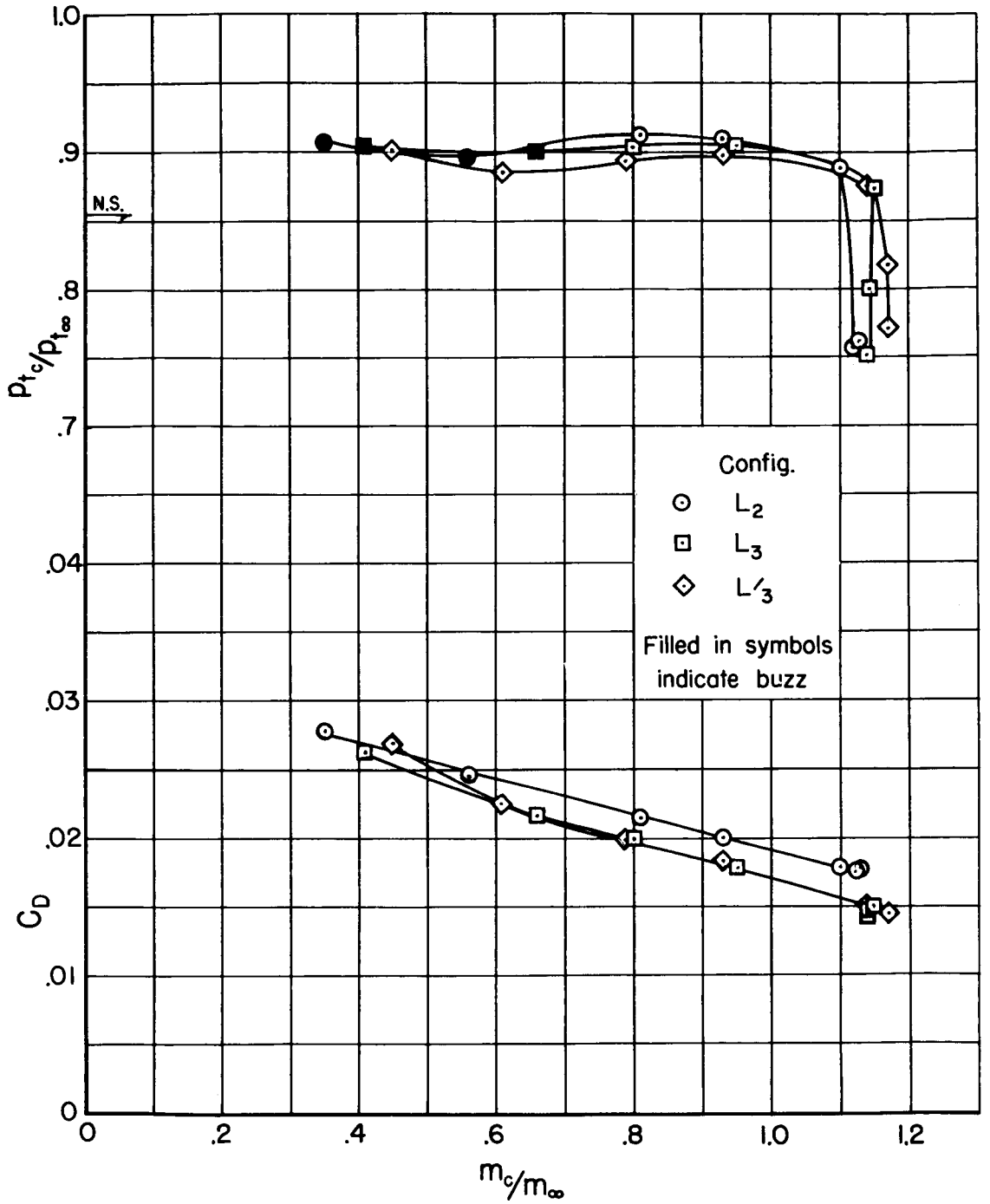

(e) $M_\infty = 1.7$; $\alpha = 0.85^\circ$

Figure 8.- Continued.

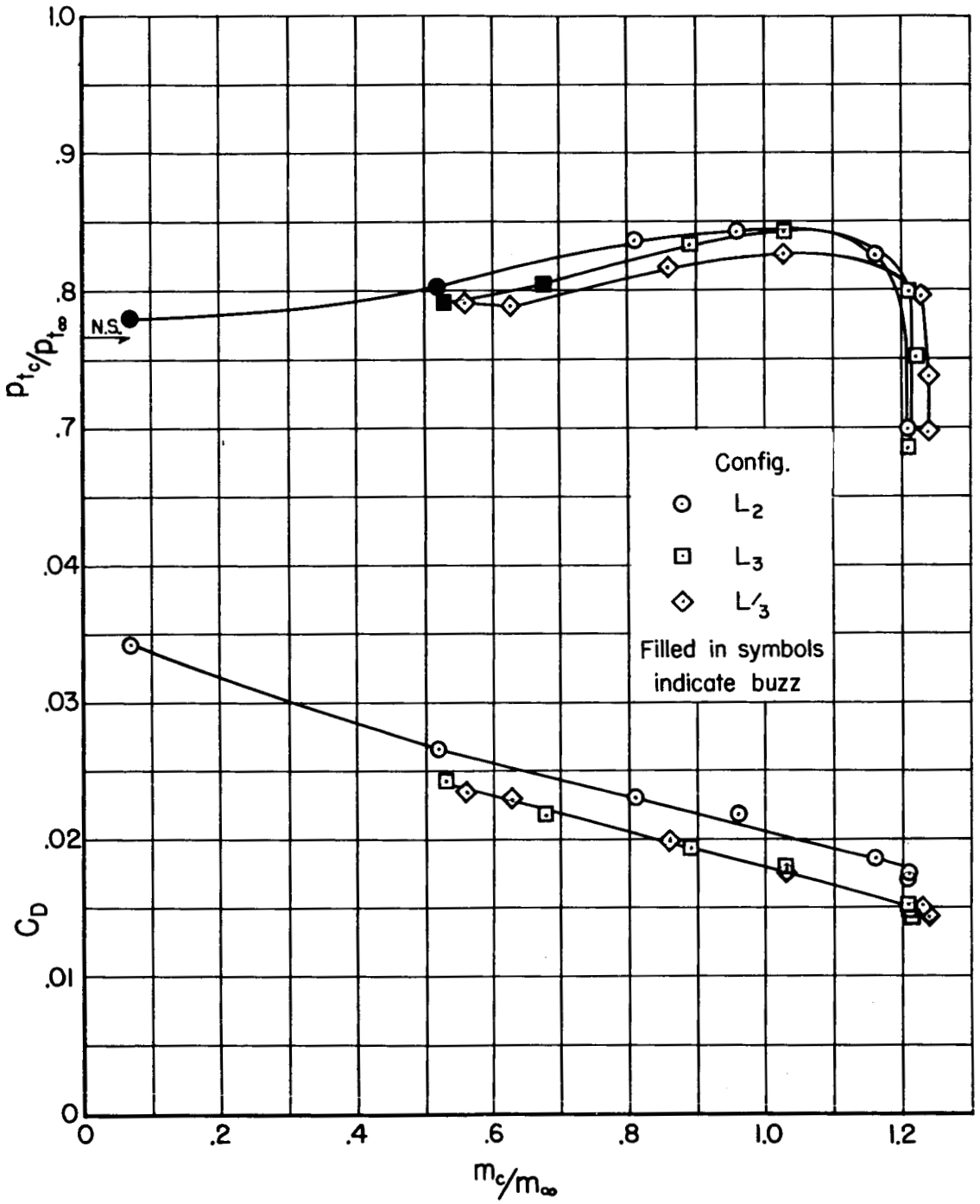

(f) $M_\infty = 1.9$; $\alpha = 0.85^\circ$

Figure 8.- Concluded.

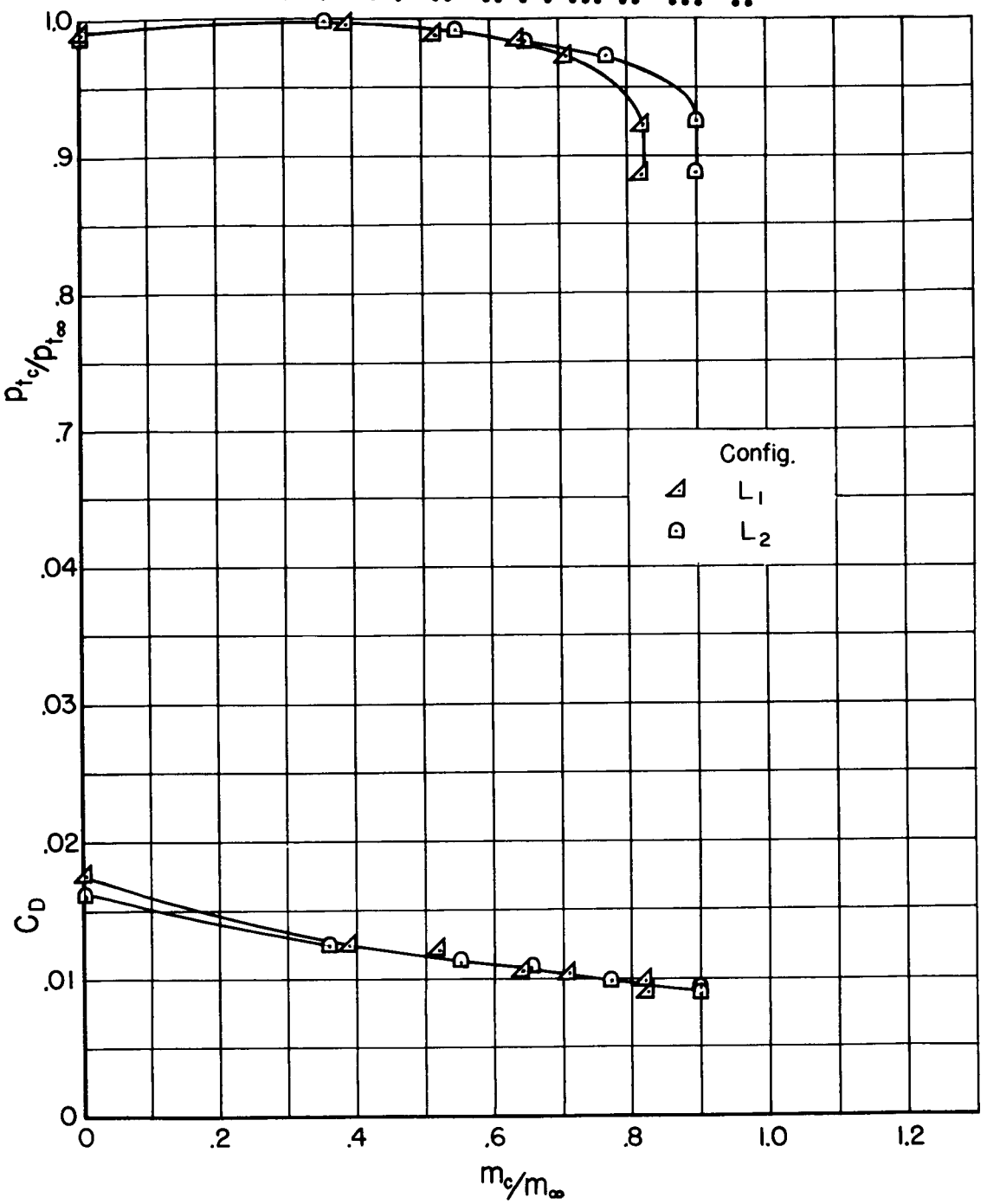

(a) $M_\infty = 0.9$; $\alpha = 7.6^\circ$

Figure 9.- Effect of lip shape on the pressure recovery and drag with nose number 5.

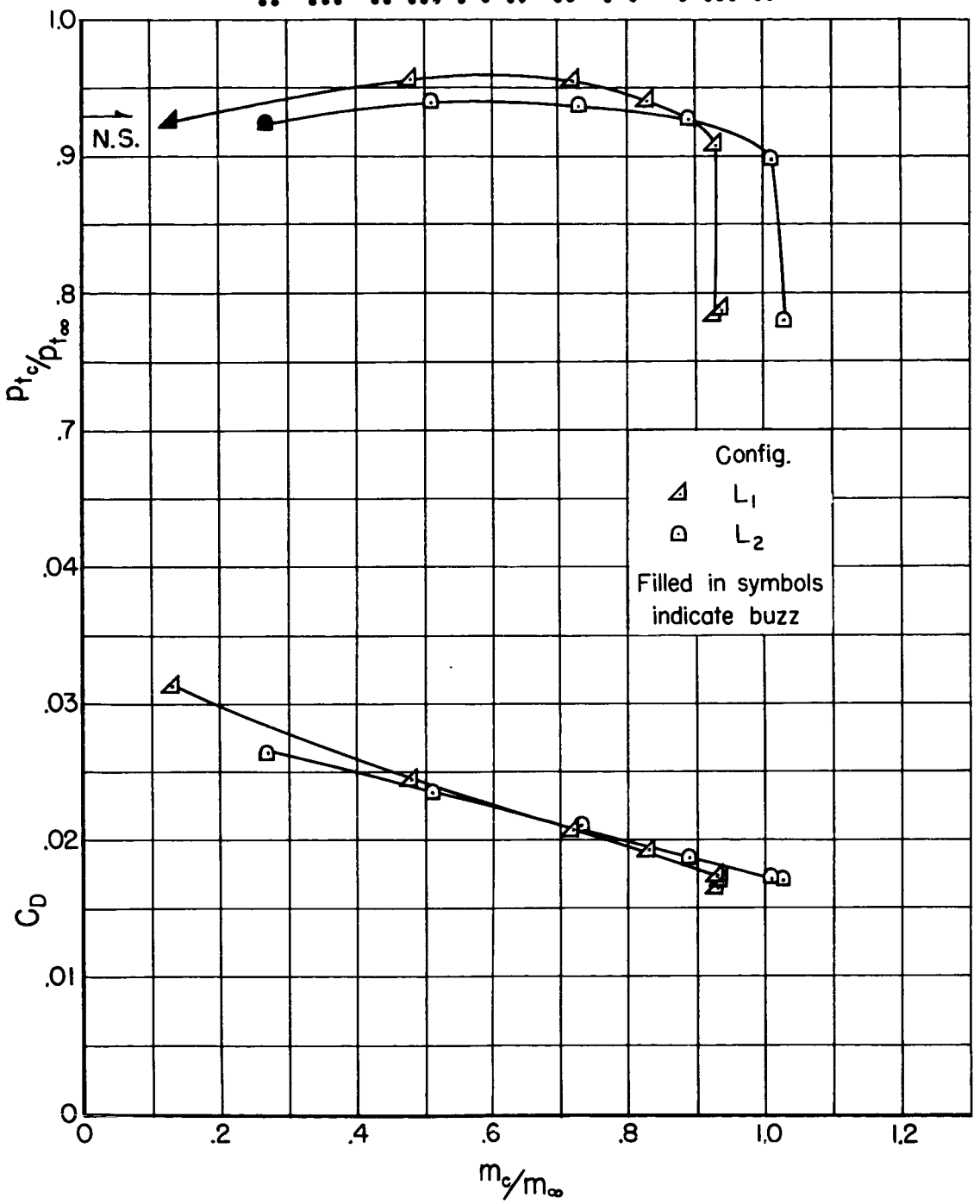

(b) $M_\infty = 1.5$; $\alpha = 3.0^\circ$

Figure 9.- Concluded.

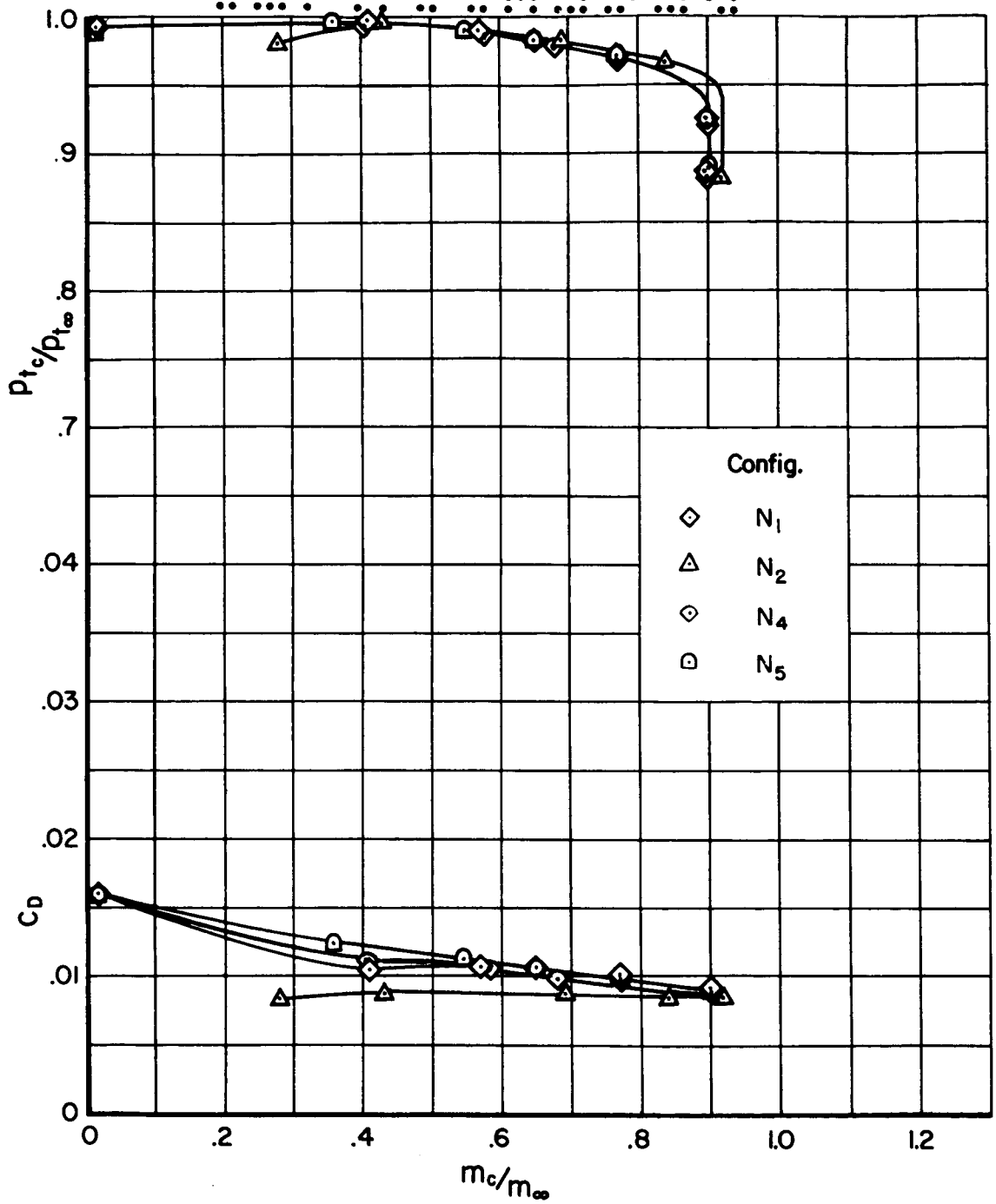

(a) $M_\infty = 0.9$; $\alpha = 7.6^\circ$

Figure 10.- Effect of nose shape on the pressure recovery and drag with lip number 2.

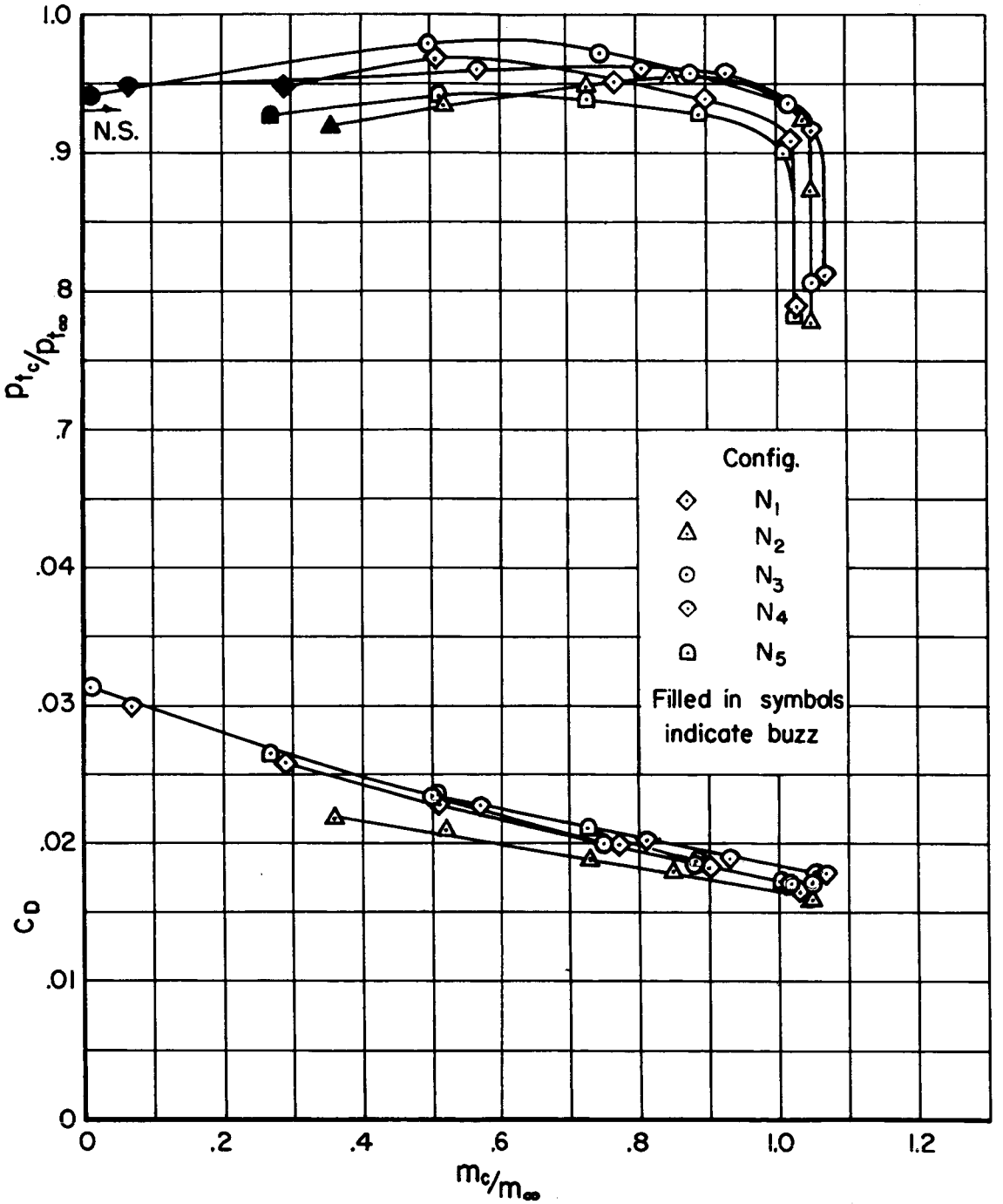

(b) $M_\infty = 1.5$; $\alpha = 3.0^\circ$

Figure 10.- Continued.

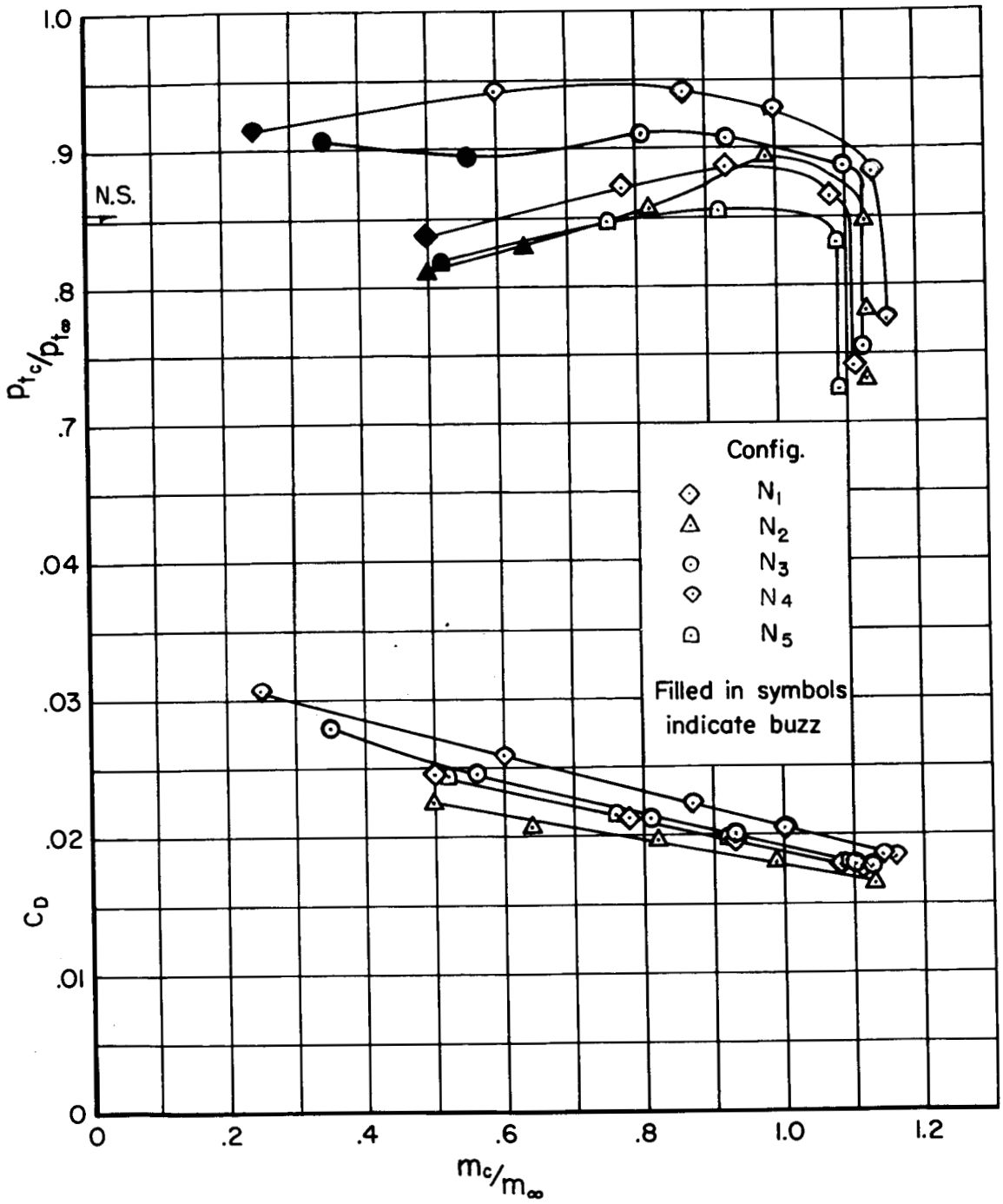

(c) $M_\infty = 1.7$; $\alpha = 0.85^\circ$

Figure 10.- Continued.

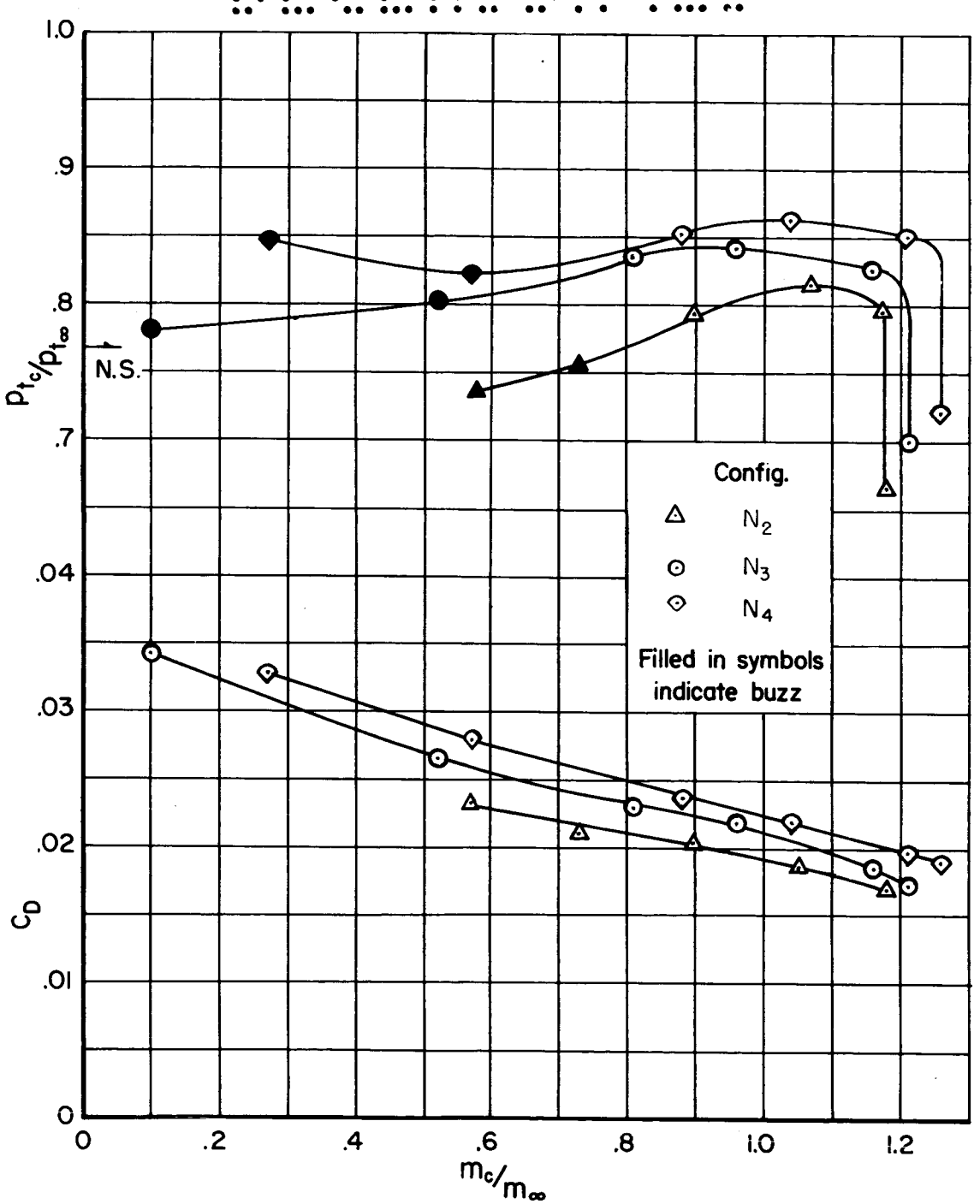

(d) $M_\infty = 1.9$; $\alpha = 0.9^\circ$

Figure 10.- Concluded.

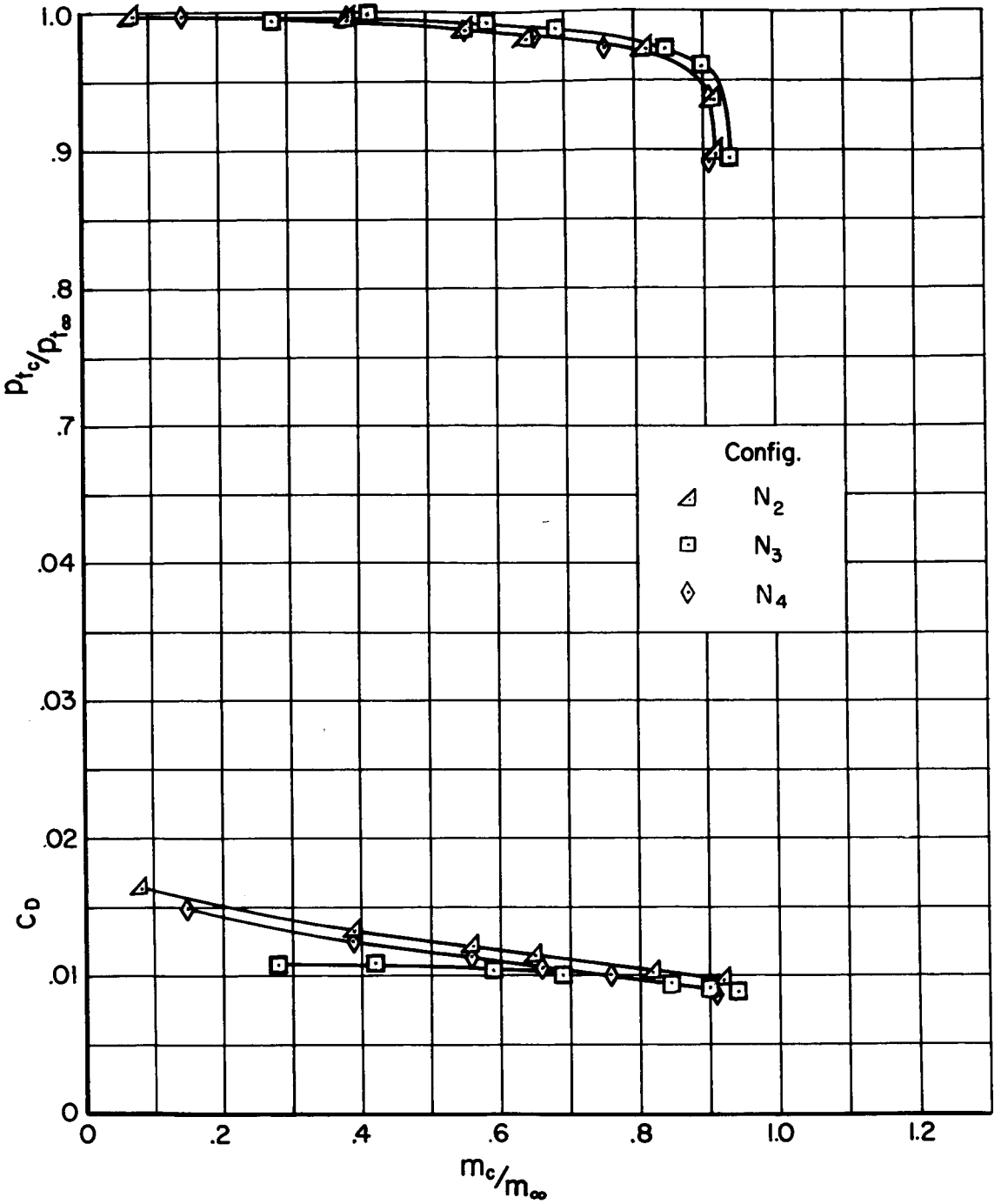

(a) $M_\infty = 0.9$; $\alpha = 7.6^\circ$

Figure 11.- Effect of nose shape on the pressure recovery and drag with lip number 3.

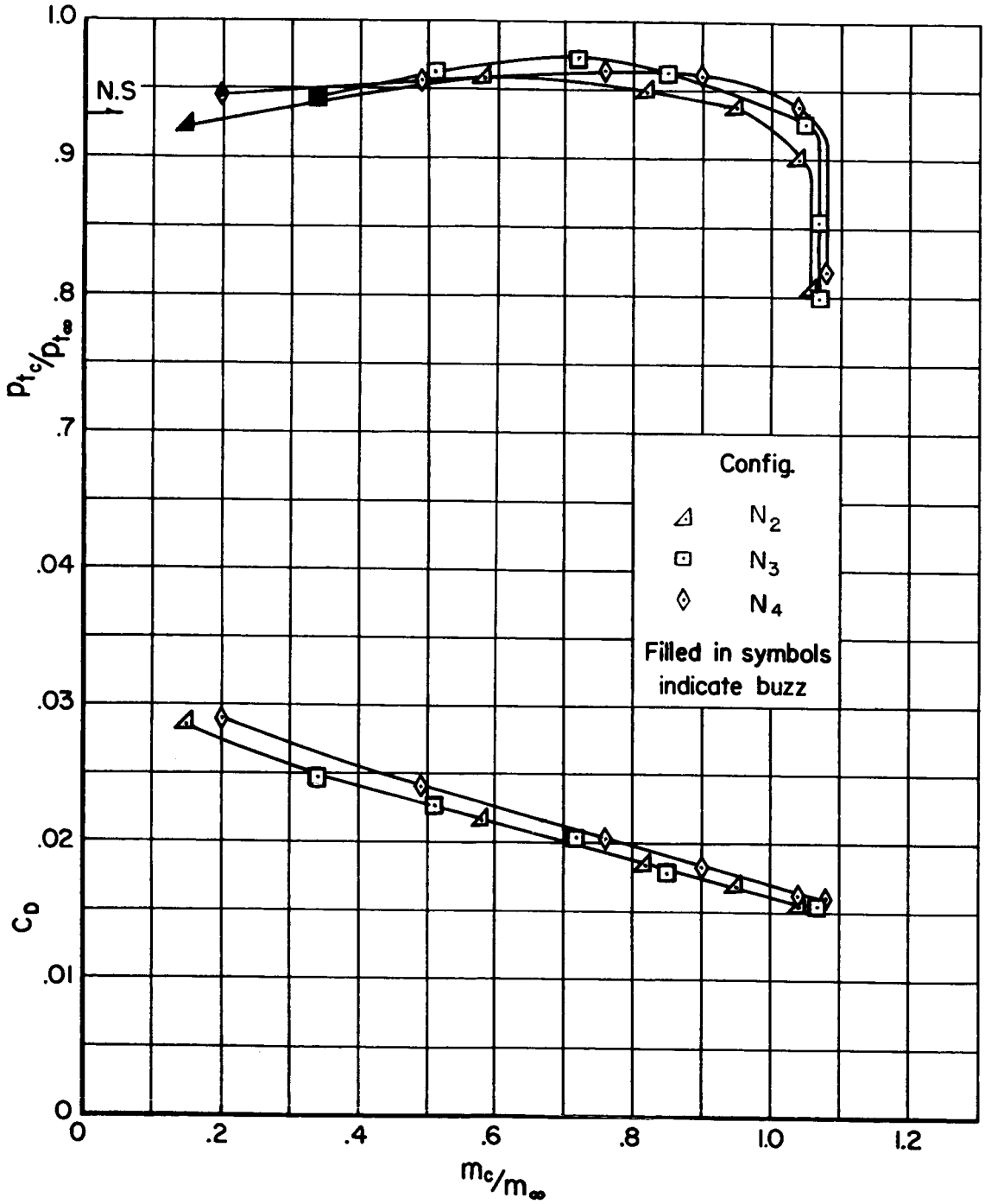

(b) $M_\infty = 1.5$; $\alpha = 3.0^\circ$

Figure 11.- Continued.

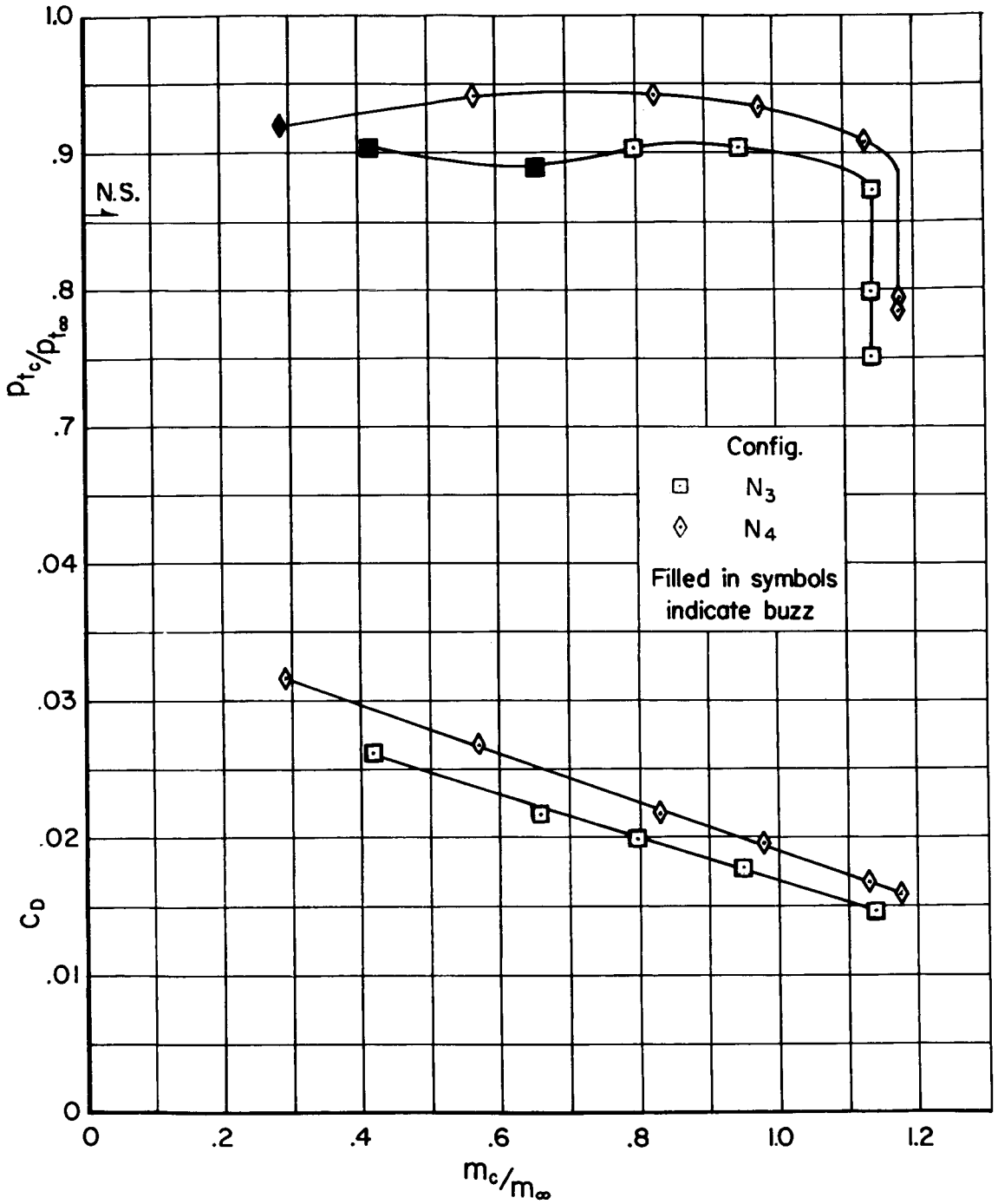

(c) $M_\infty = 1.7$; $\alpha = 0.85^\circ$

Figure 11.- Concluded.

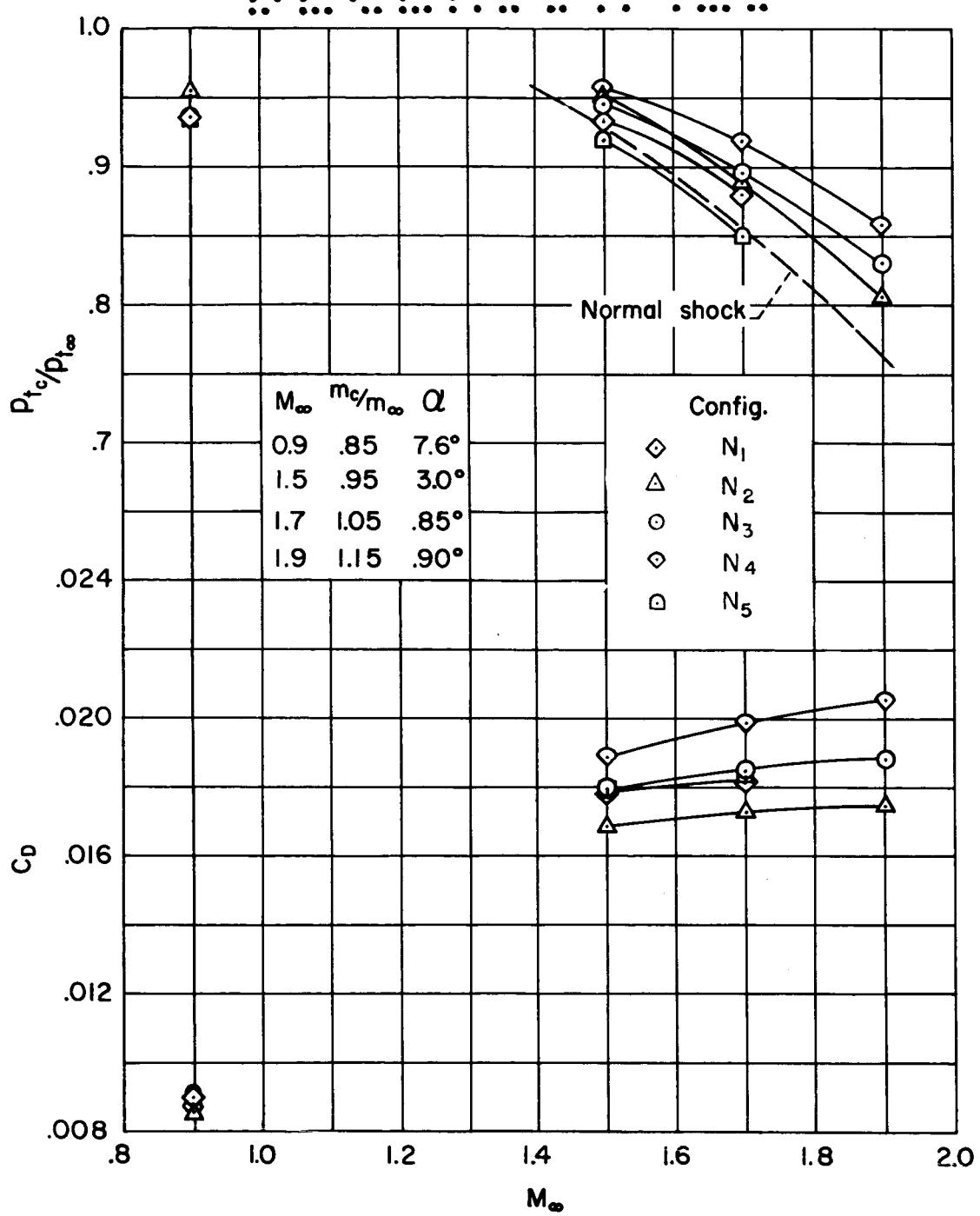

(a) Lip shape 2.

Figure 12.- Effect of nose shapes on the pressure recovery and drag at mass-flow ratios for typical inlet-engine matched conditions.

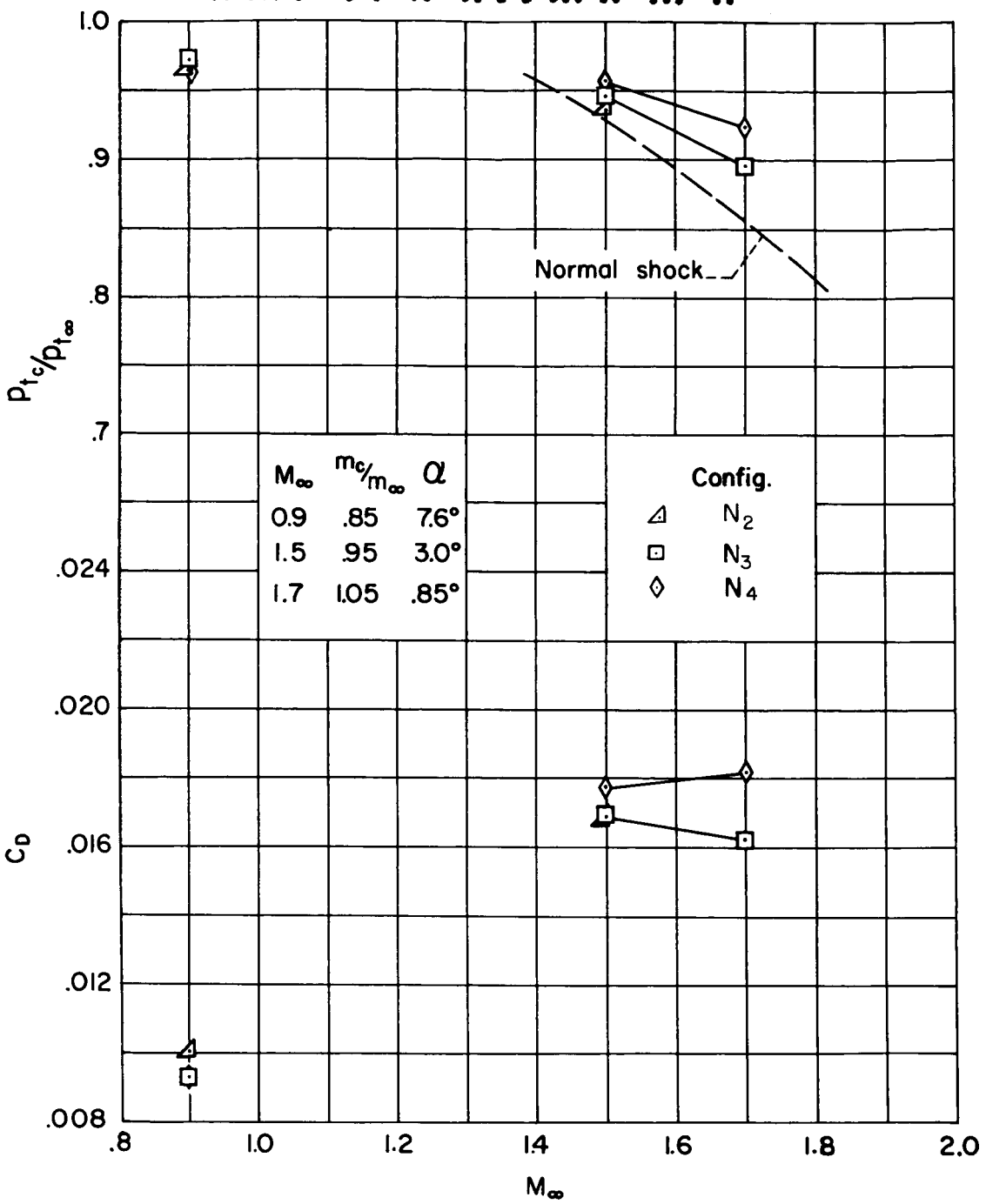

(b) Lip shape 3.

Figure 12.- Concluded.

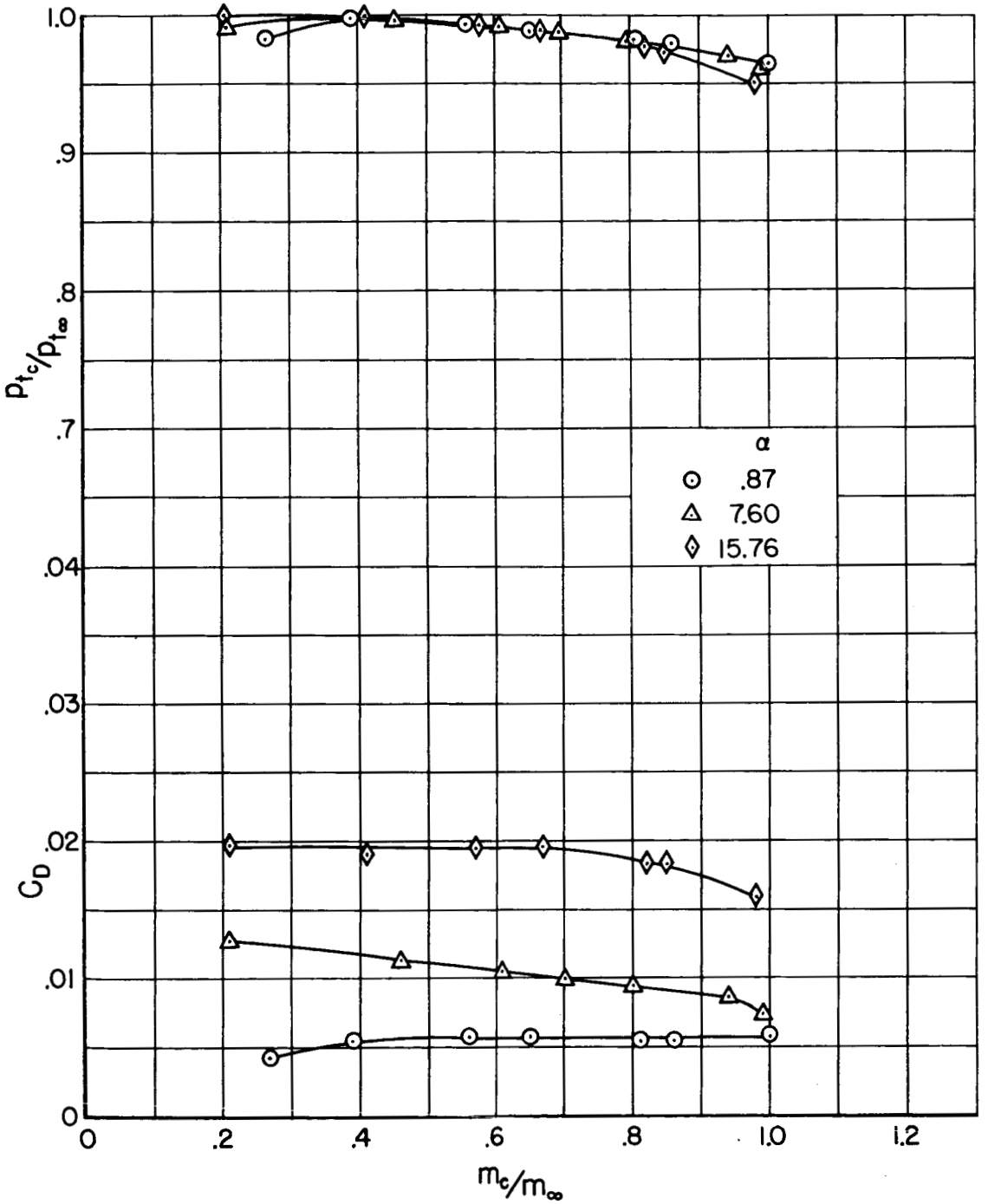

(a) $M_\infty = 0.6$

Figure 13.- The effect of angle of attack on the pressure recovery and drag for configuration N_2L_2.

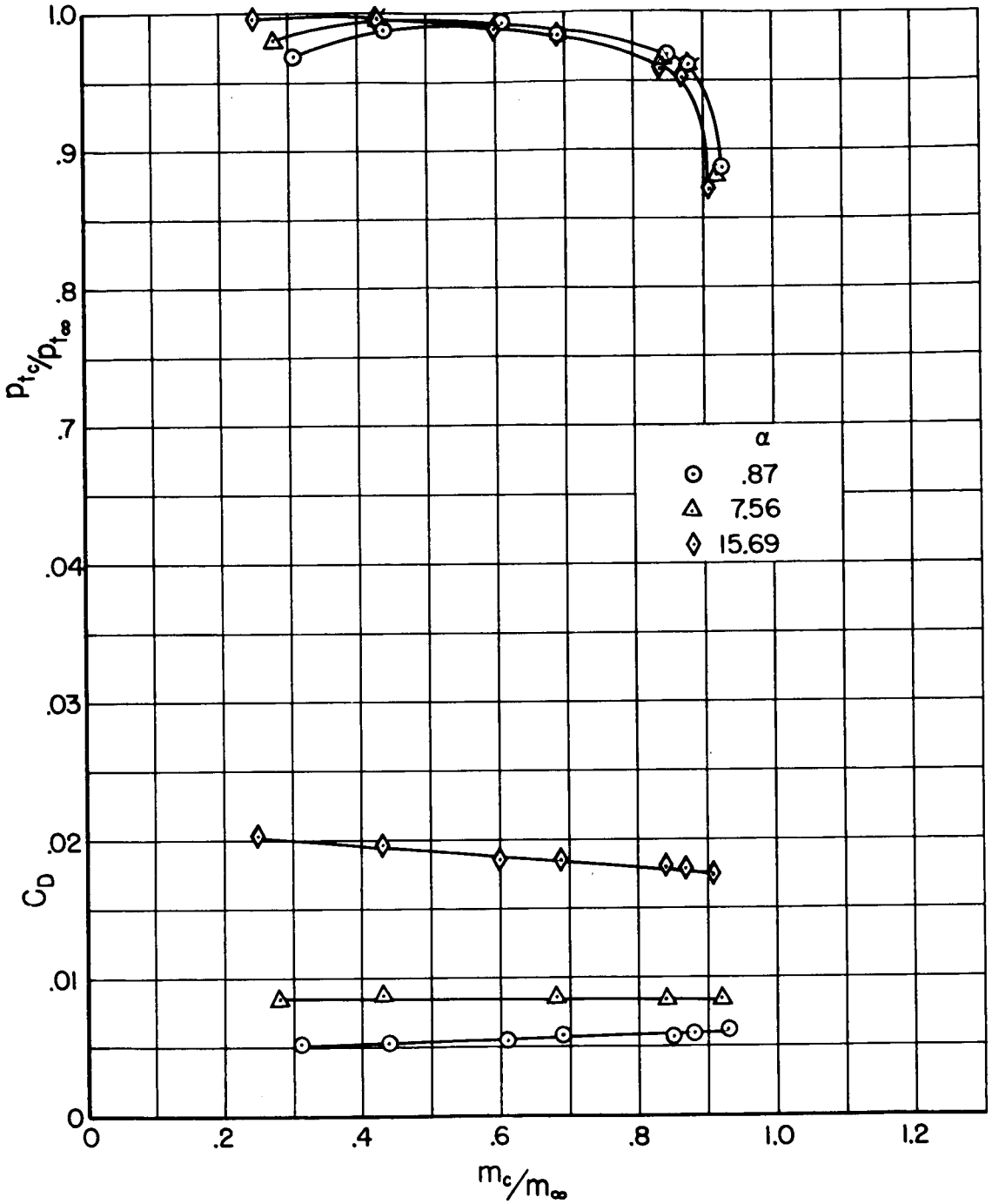

(b) $M_\infty = 0.9$

Figure 13.- Continued.

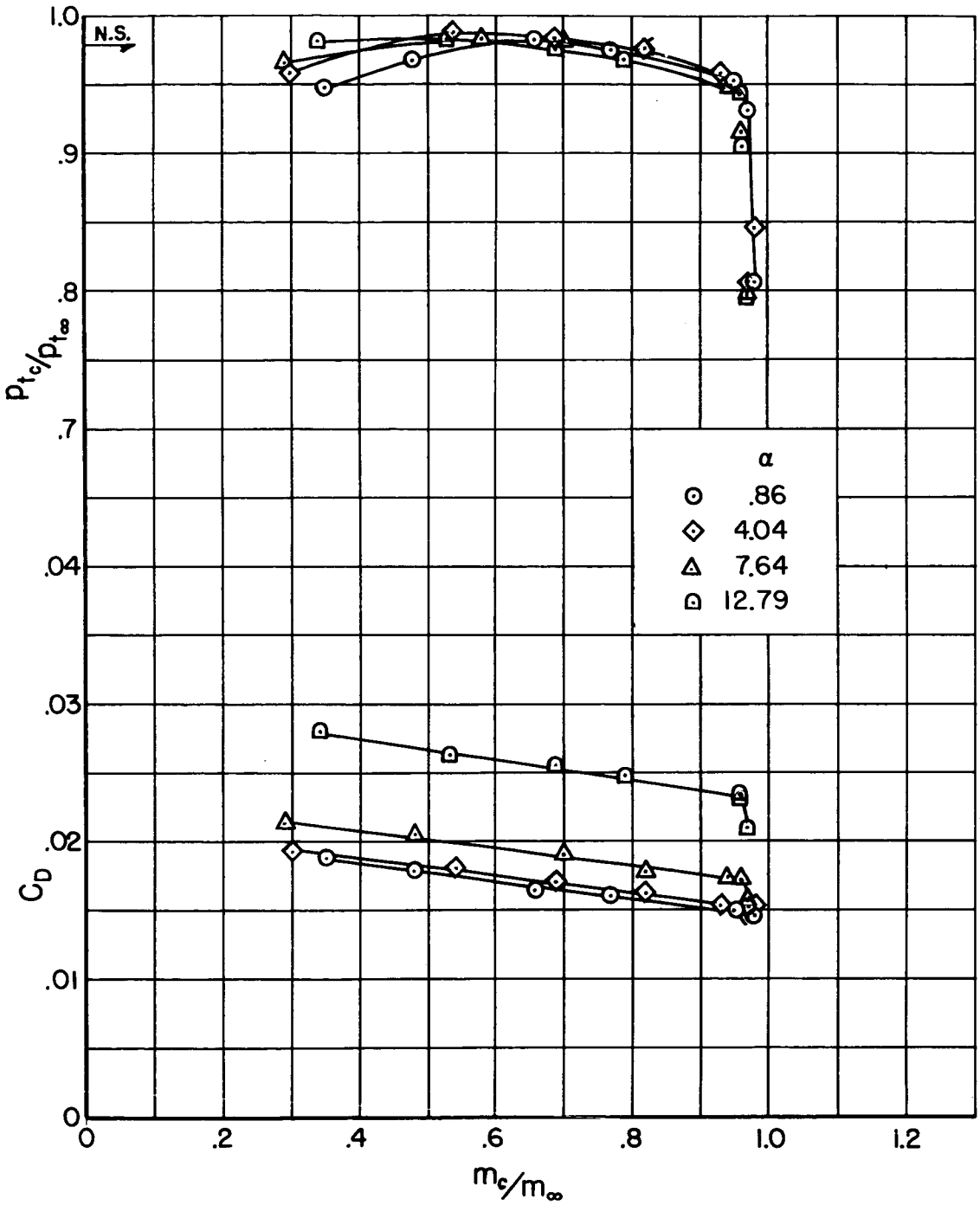

(c) $M_\infty = 1.3$

Figure 13.- Continued.

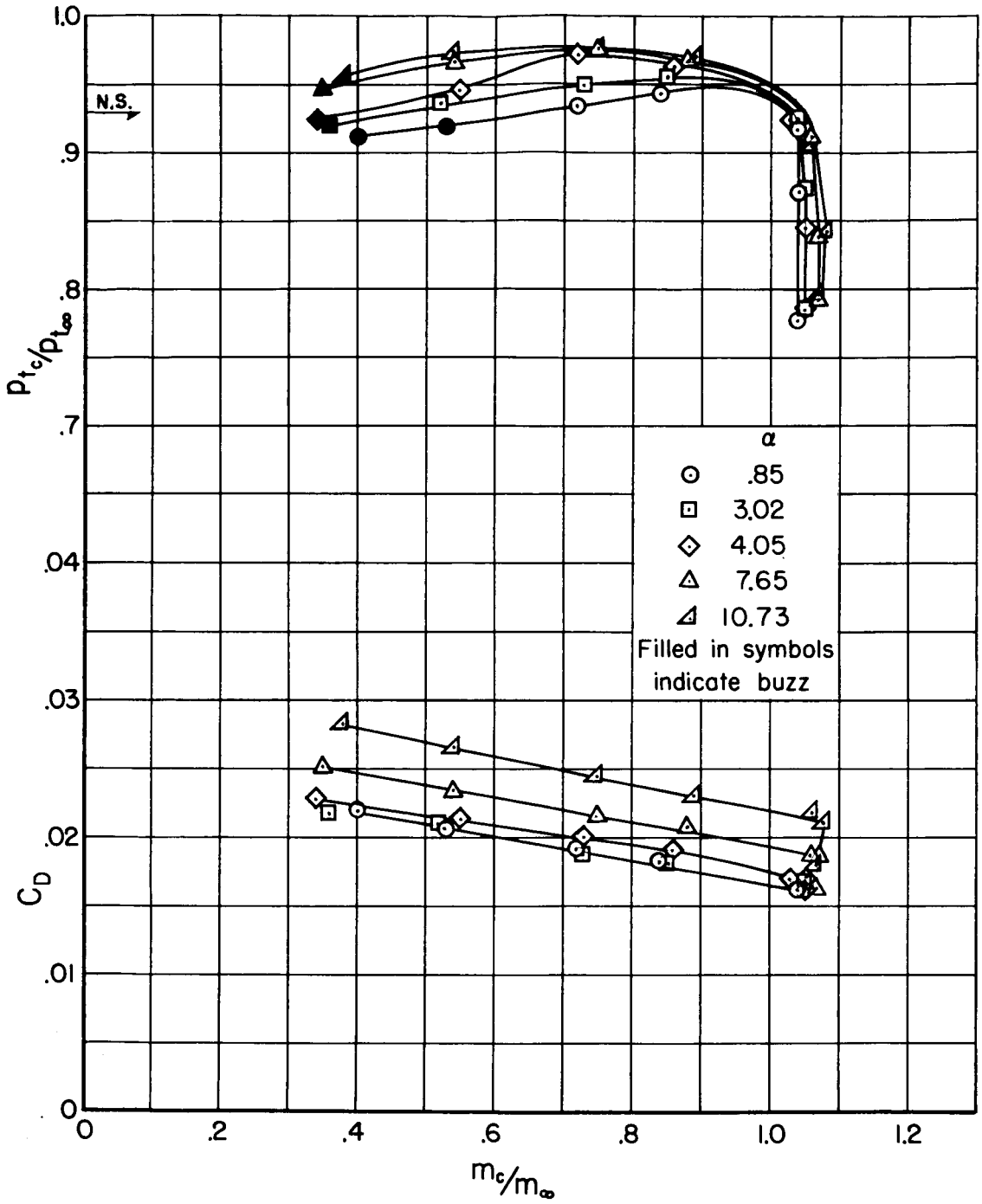

(d) $M_\infty = 1.5$

Figure 13.- Continued.

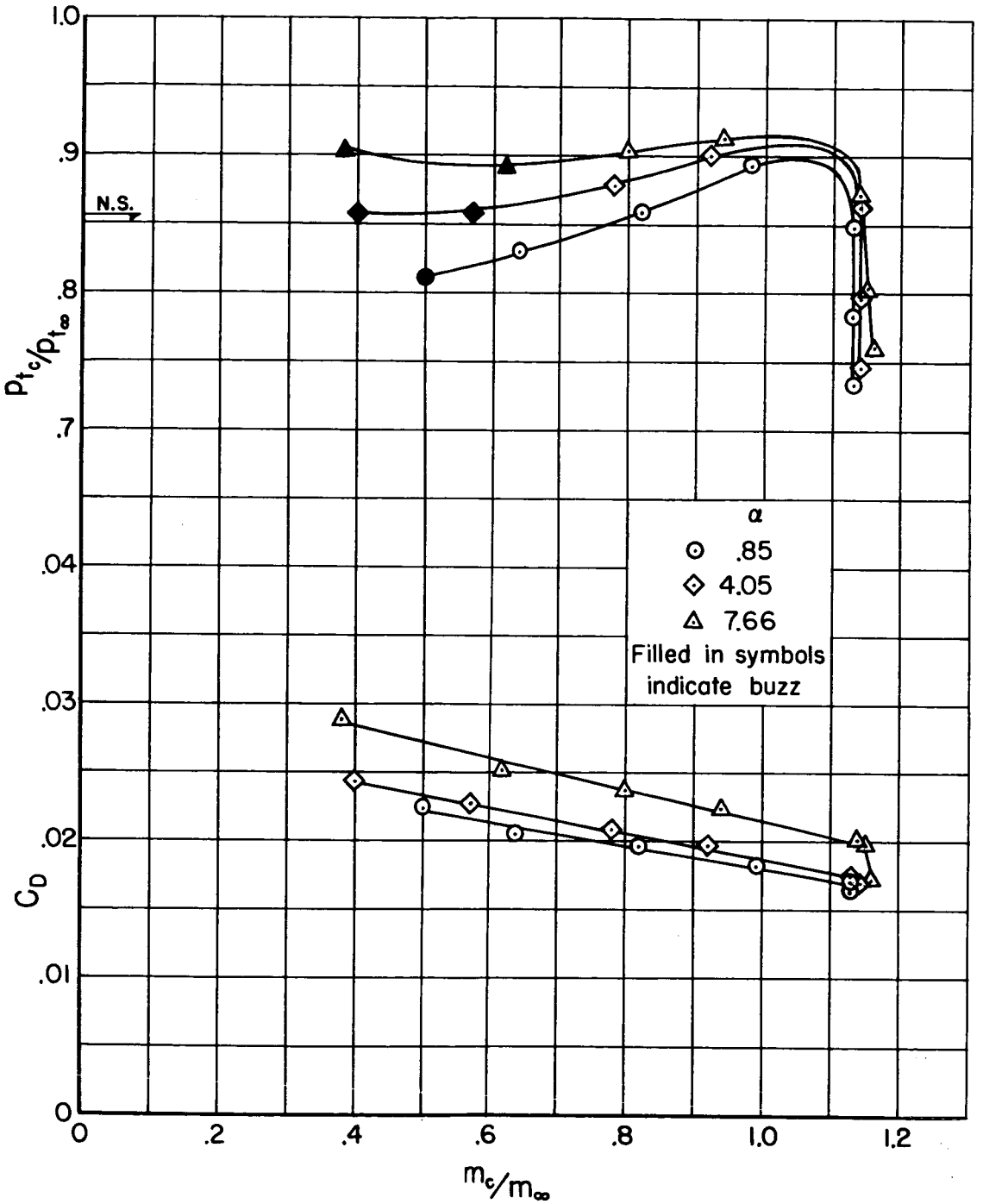

(e) $M_\infty = 1.7$

Figure 13.- Continued.

[redacted]

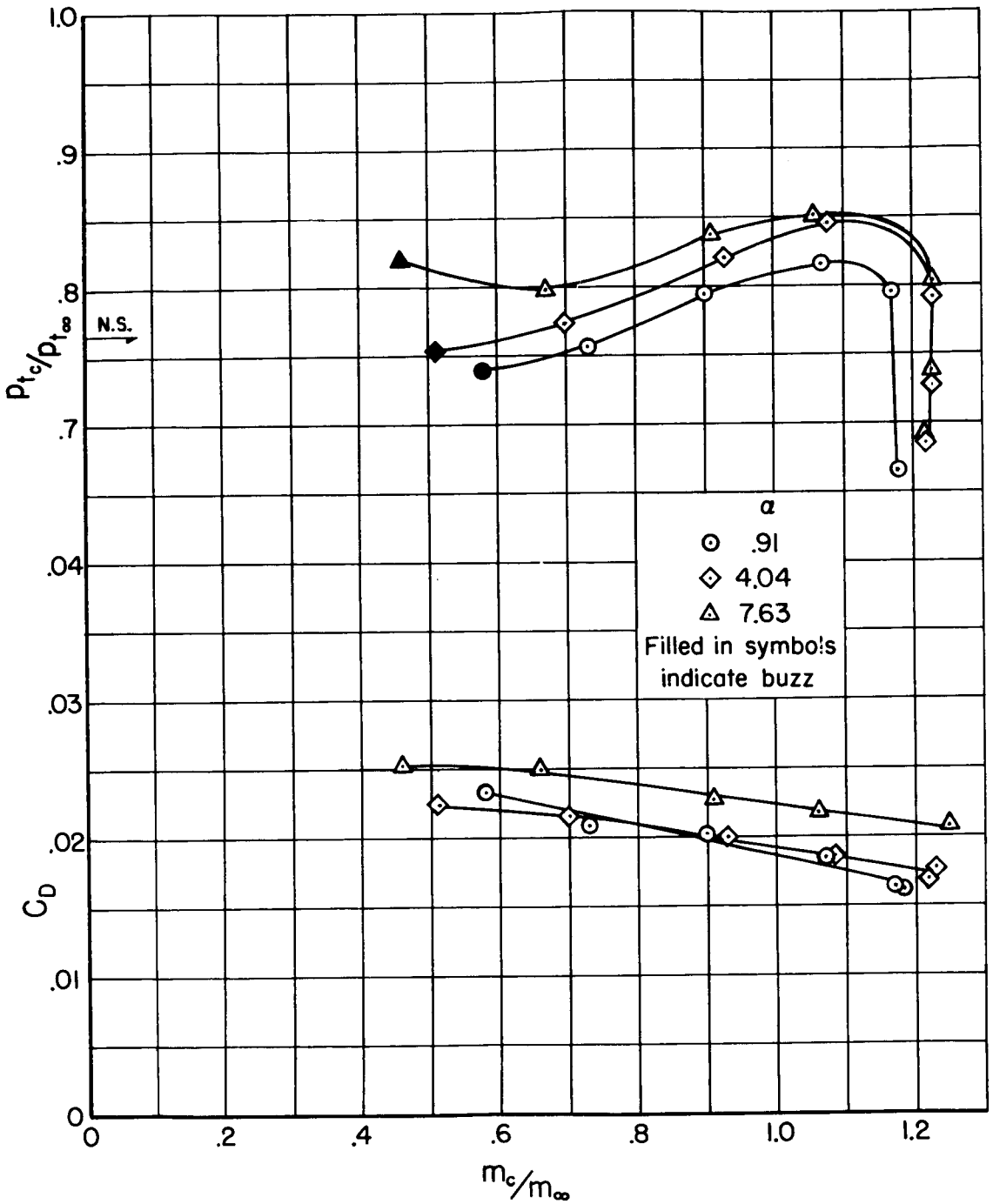

(f) $M_\infty = 1.9$

Figure 13.- Concluded.

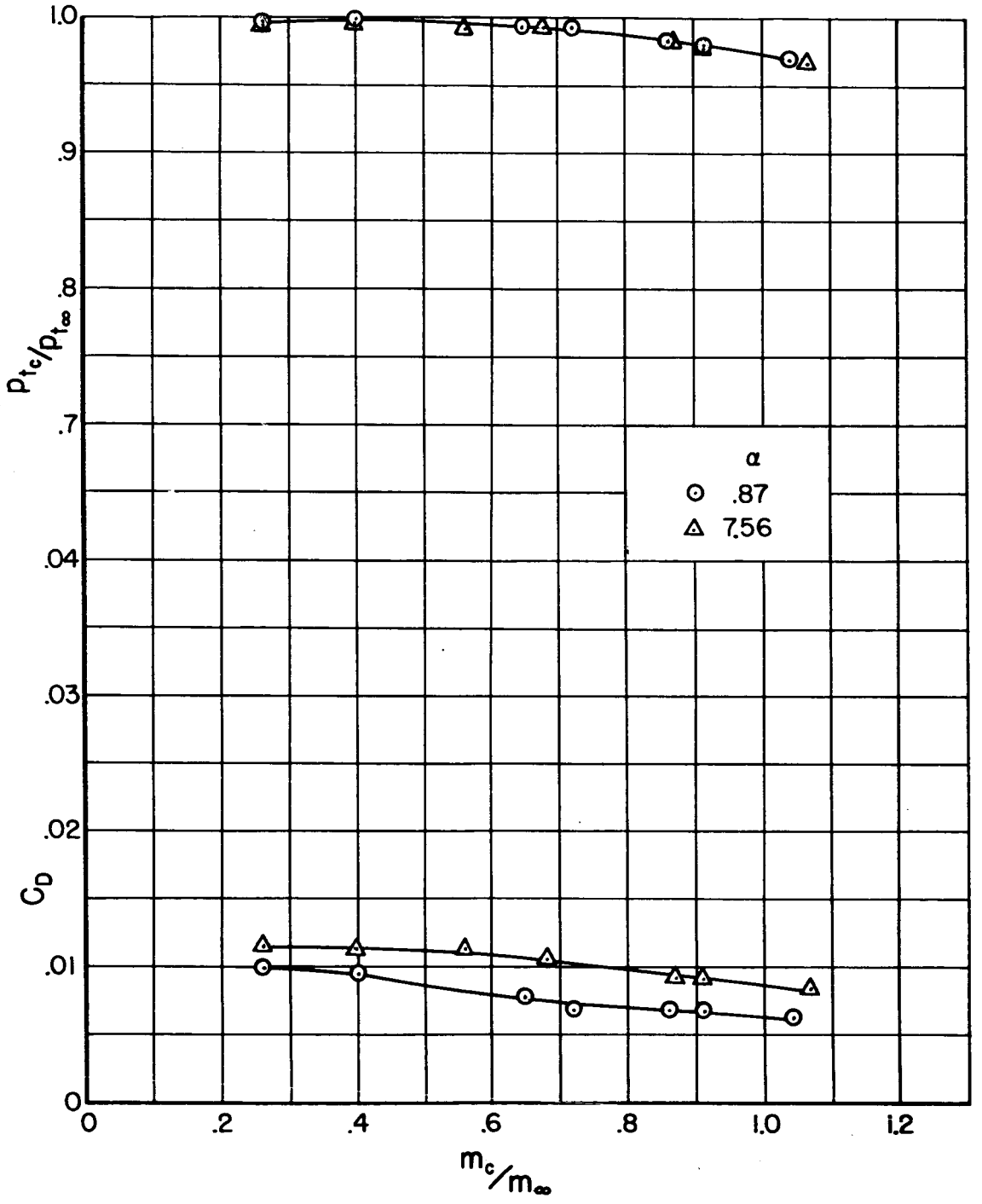

(a) $M_\infty = 0.6$

Figure 14.- The effect of angle of attack on the pressure recovery and drag for configuration $N_3L'_3$.

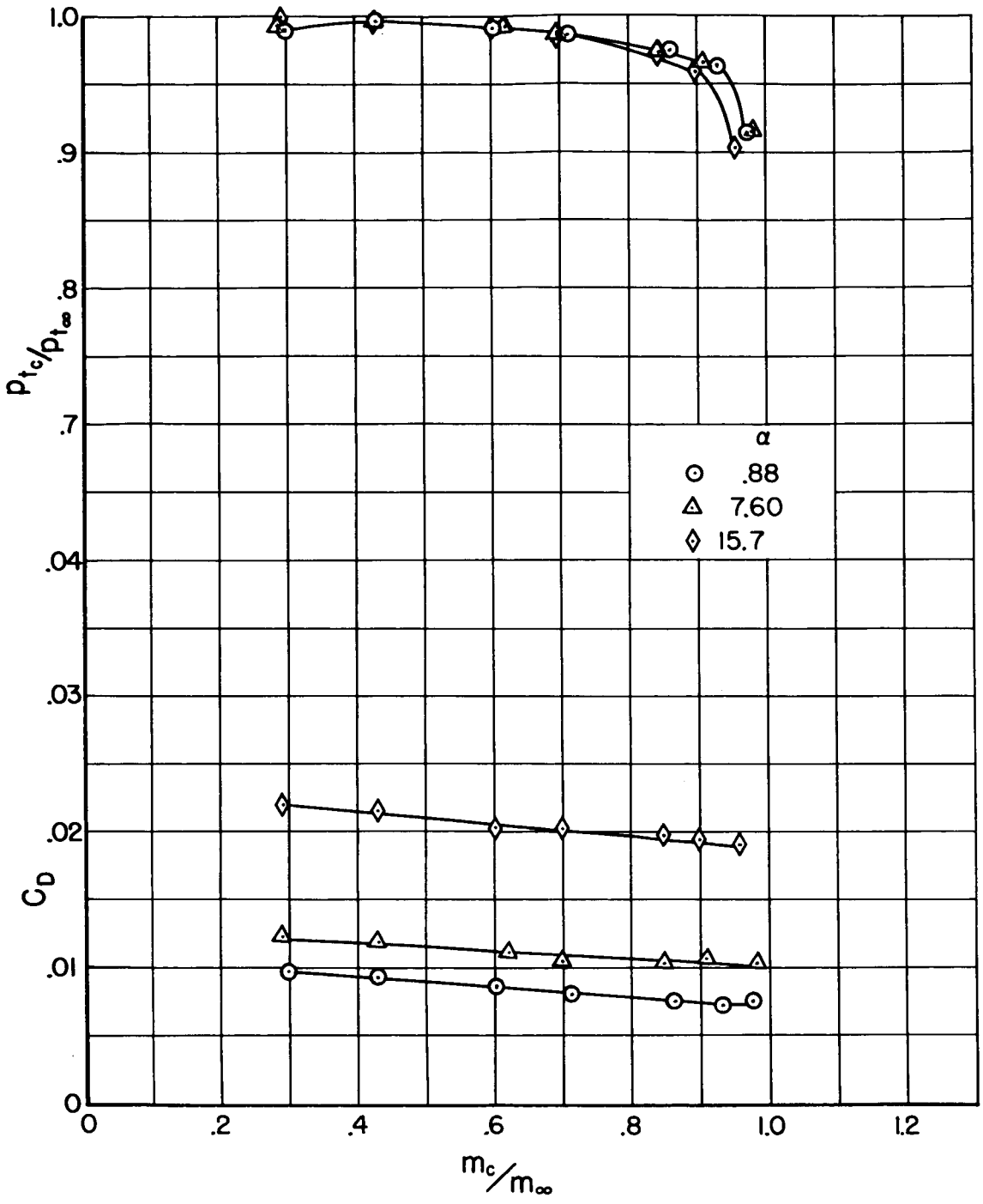

(b) $M_\infty = 0.9$

Figure 14.- Continued.

[redacted]

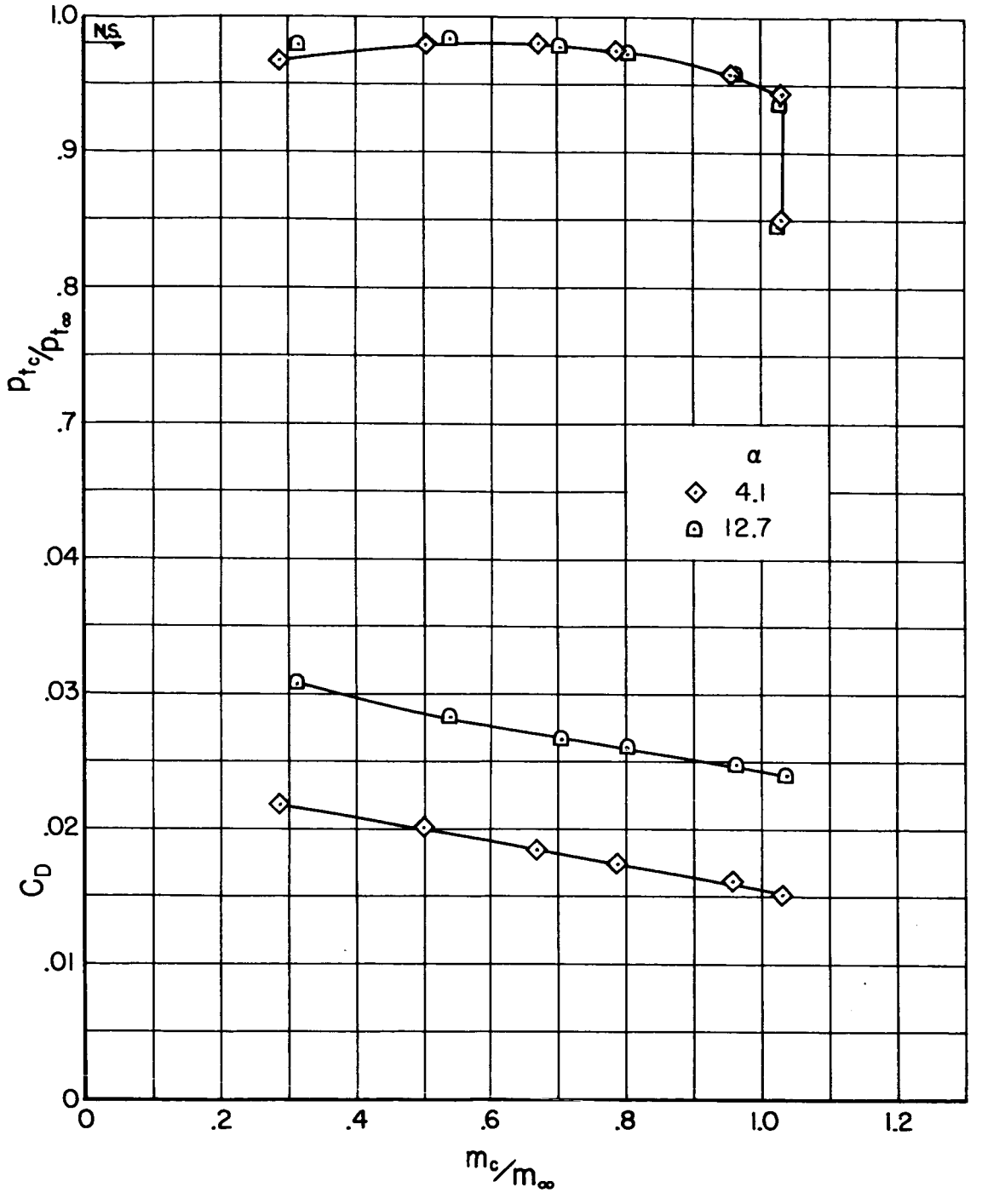

(c) $M_\infty = 1.3$

Figure 14.- Continued.

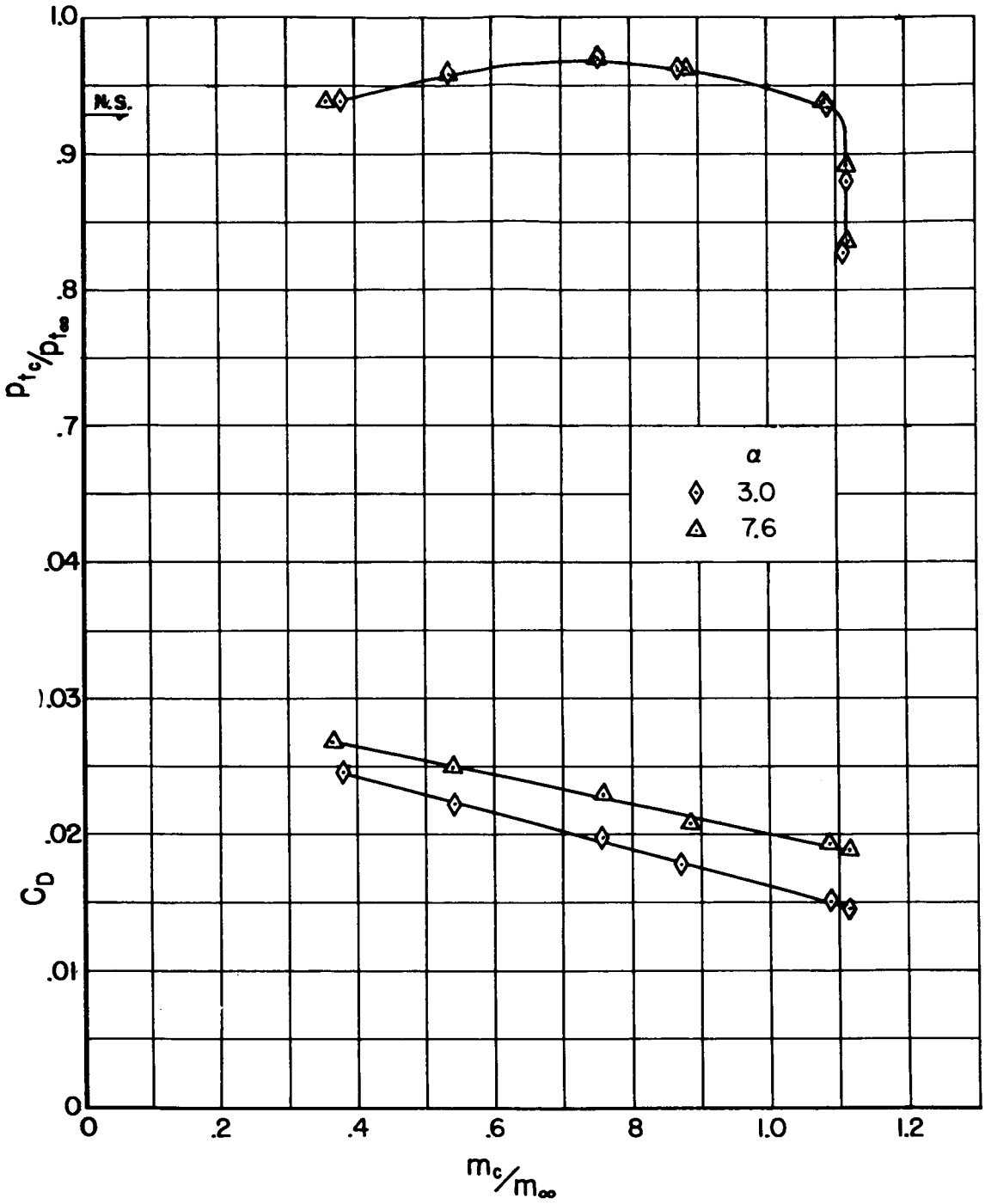

(d) $M_\infty = 1.5$

Figure 14.- Continued.

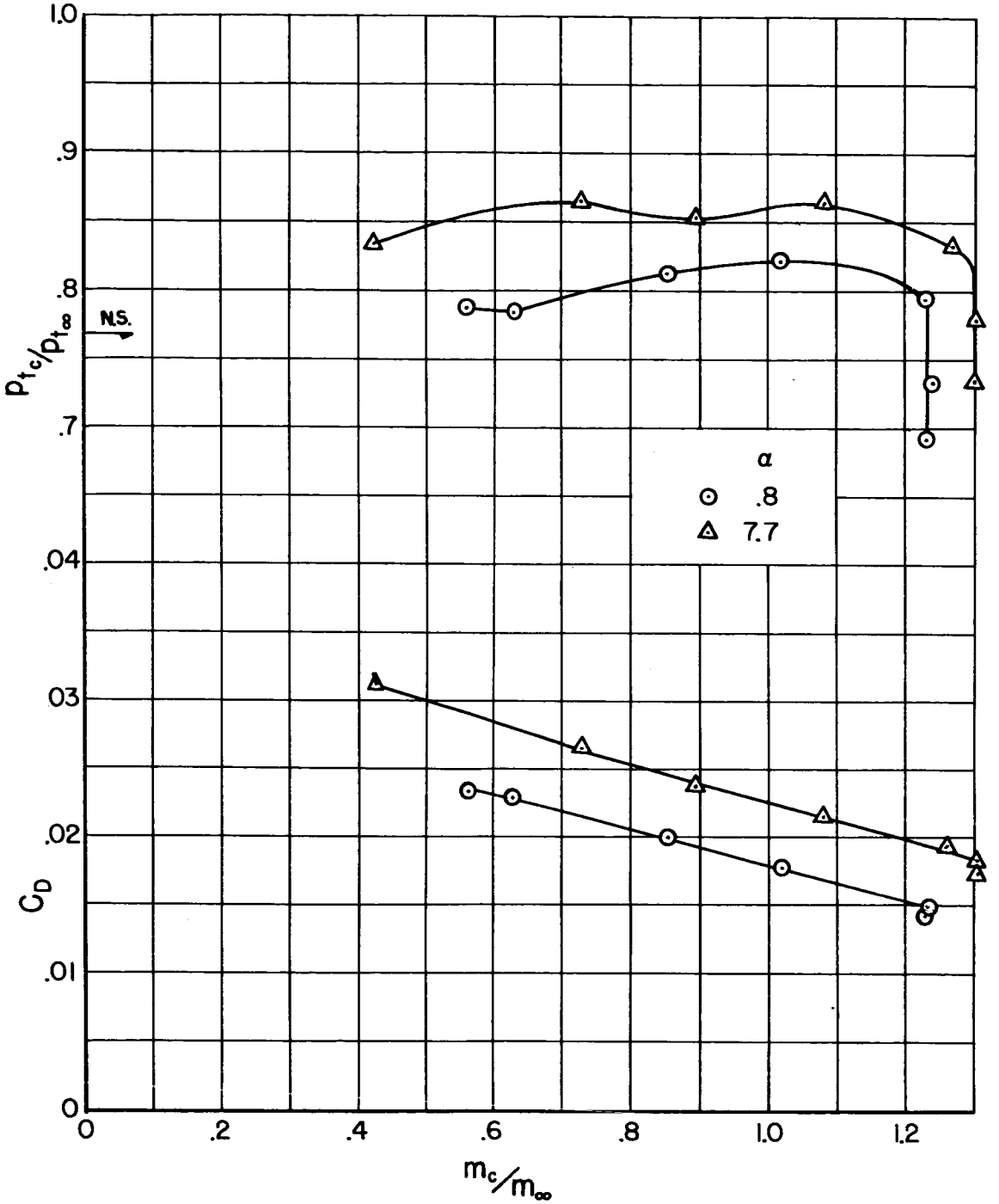

(e) $M_\infty = 1.9$

Figure 14.- Concluded.

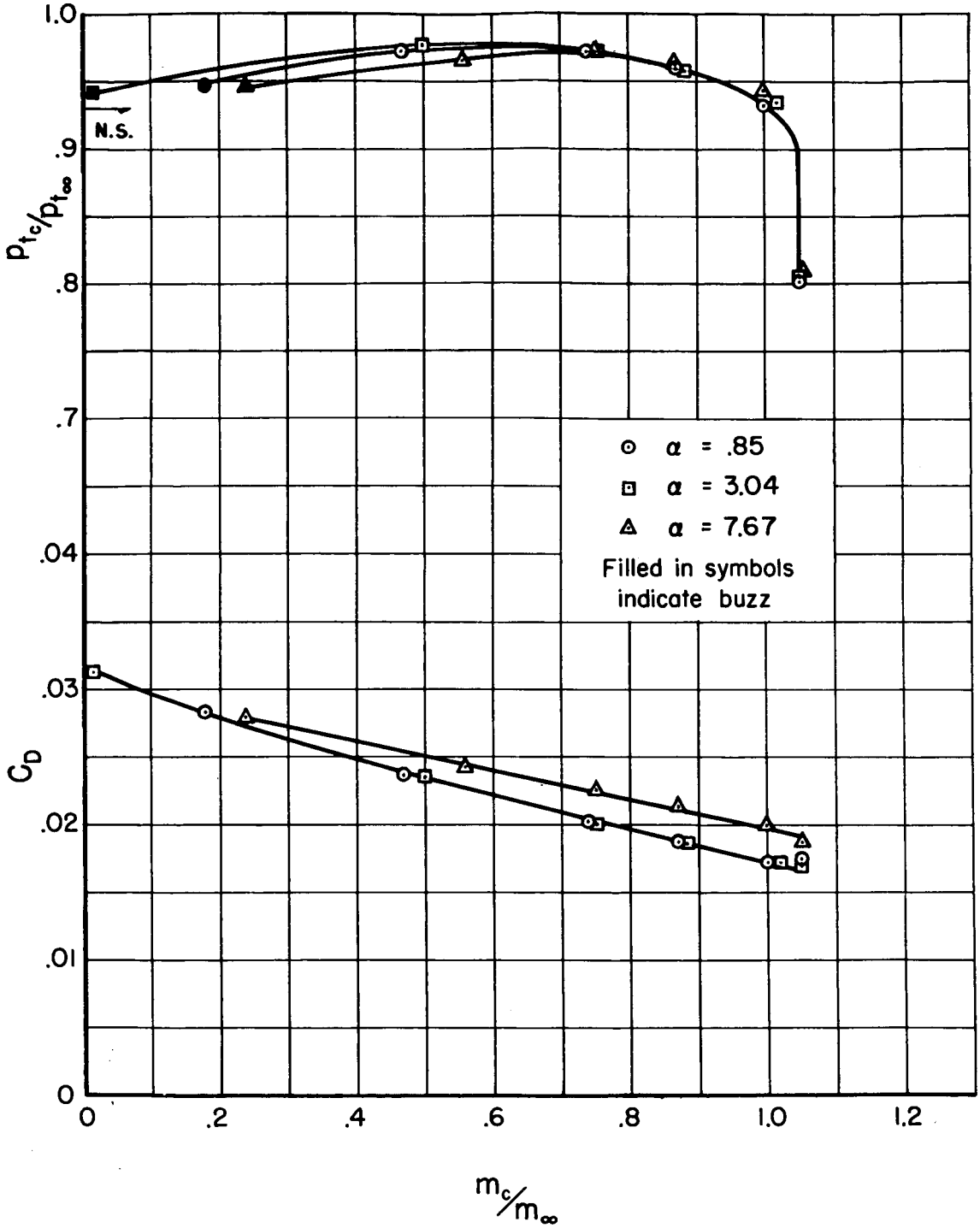

(a) $M_\infty = 1.5$

Figure 15.- The effect of angle of attack on the pressure recovery and drag for configuration N_3L_2.

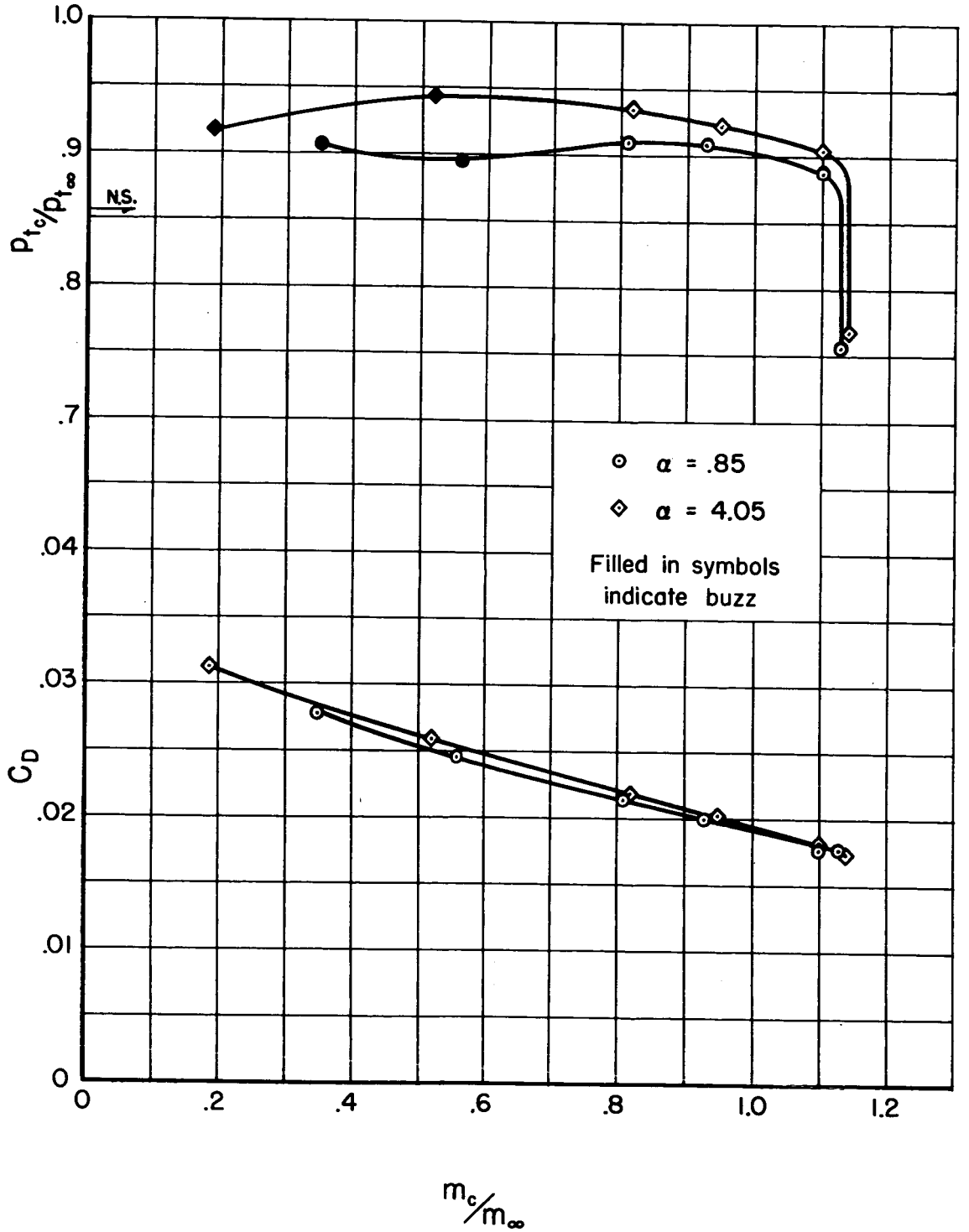

(b) $M_\infty = 1.7$

Figure 15.- Continued.

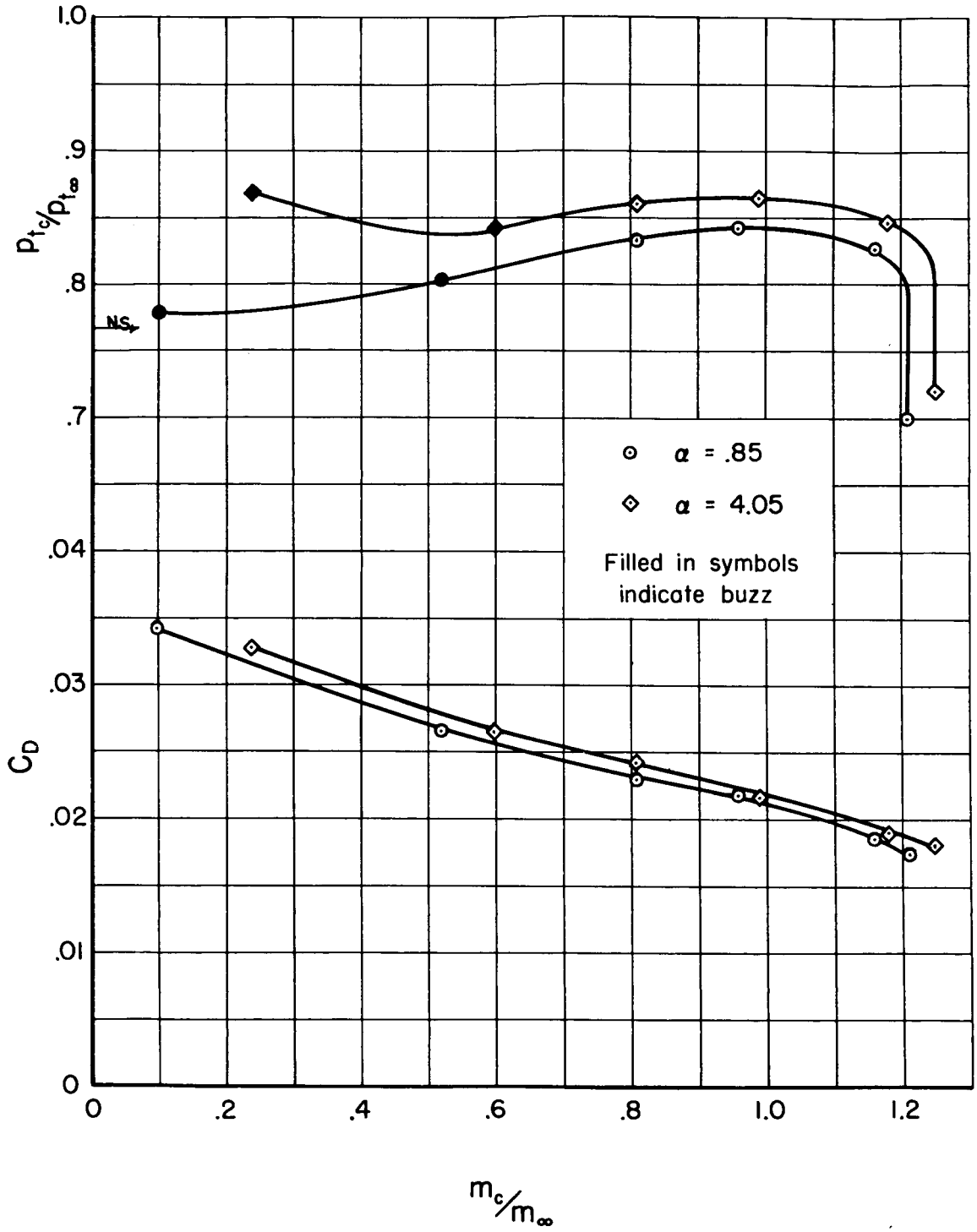

(c) $M_\infty = 1.9$

Figure 15.- Concluded.

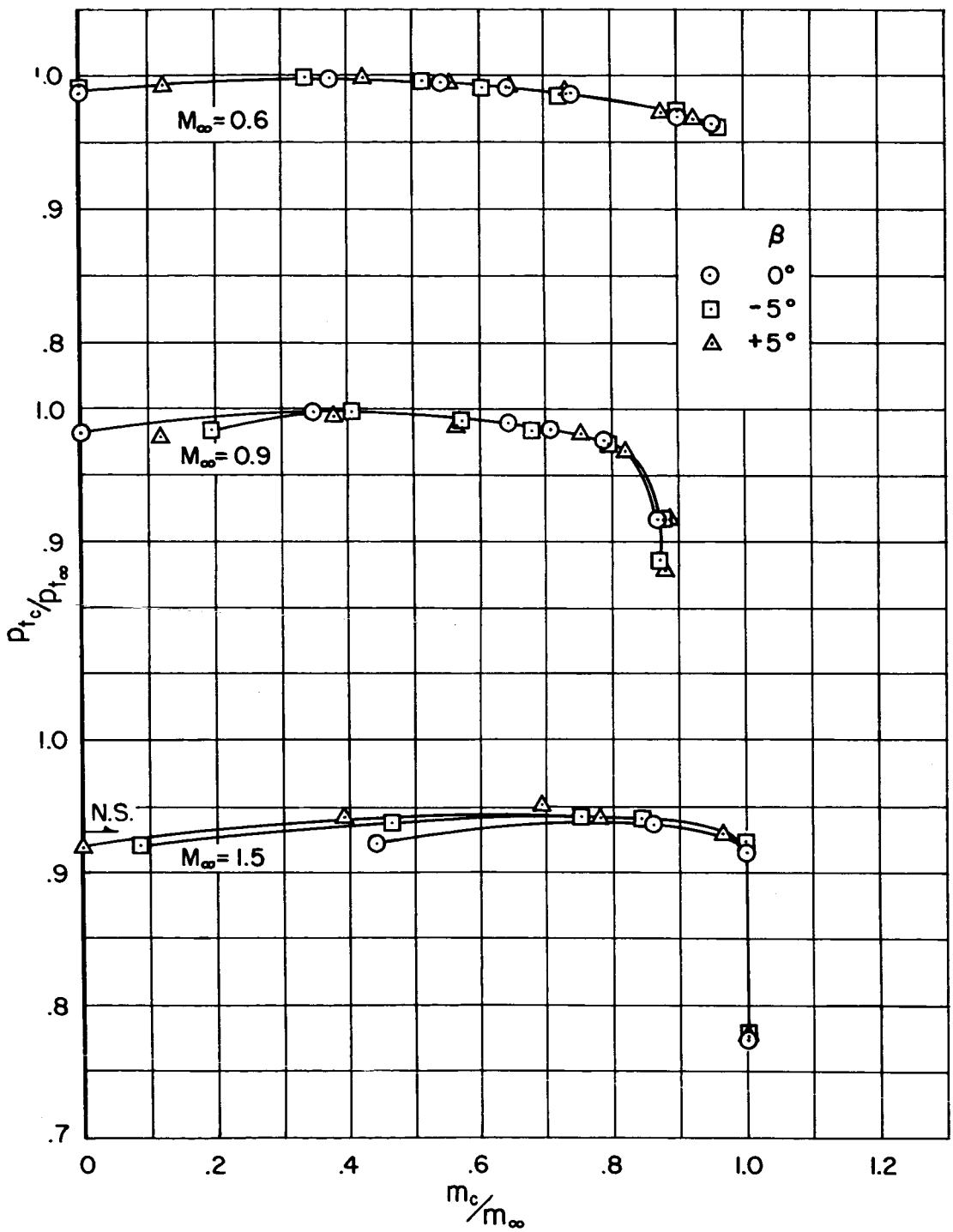

Figure 16.- The effect of angle of sideslip on pressure recovery for configuration N_2L_2; $\alpha = -0.3^\circ$.

[redacted]

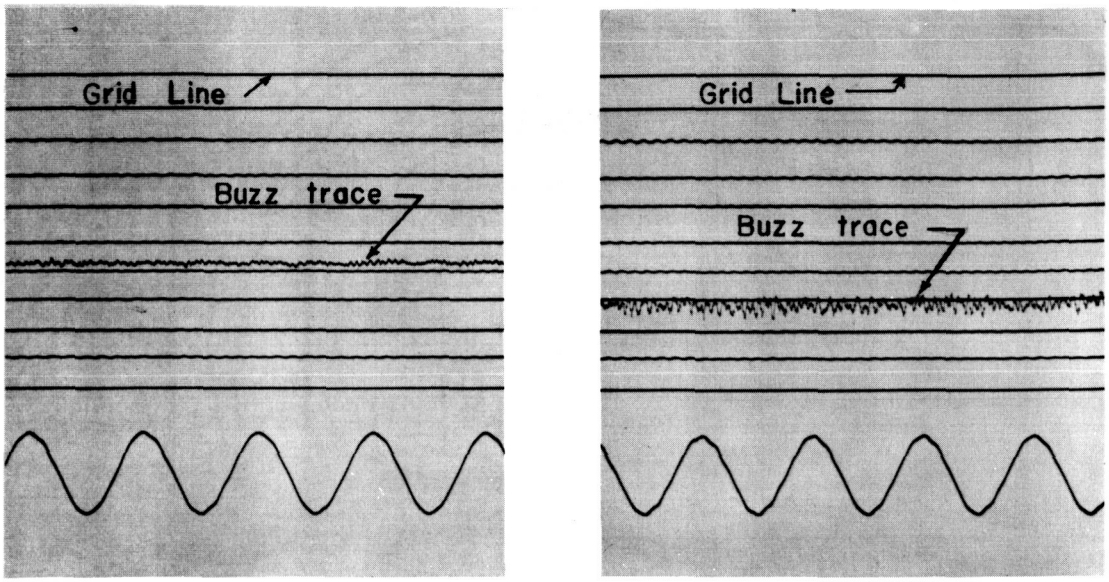

(a) No buzz, $M_c/M_\infty = 0.8$.

(b) Start of buzz, $M_c/M_\infty \cong 0.7$.

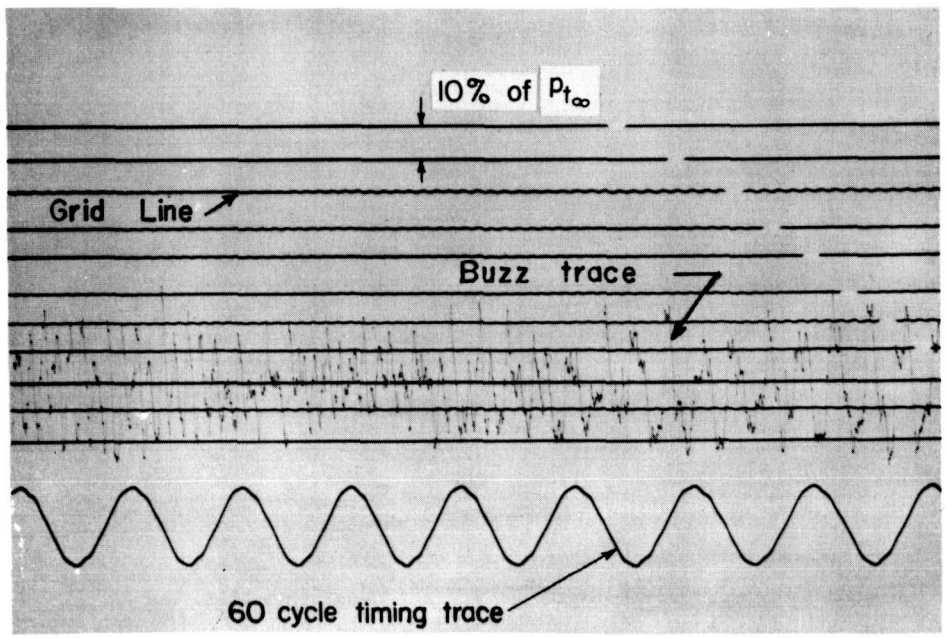

(c) Serious buzz, $M_c/M_\infty \cong 0.5$.

Figure 17.- Typical pressure-time record of inlet pressure fluctuations; configuration N_3L_3, $M_\infty = 1.9$, $\alpha = 0.85^\circ$.

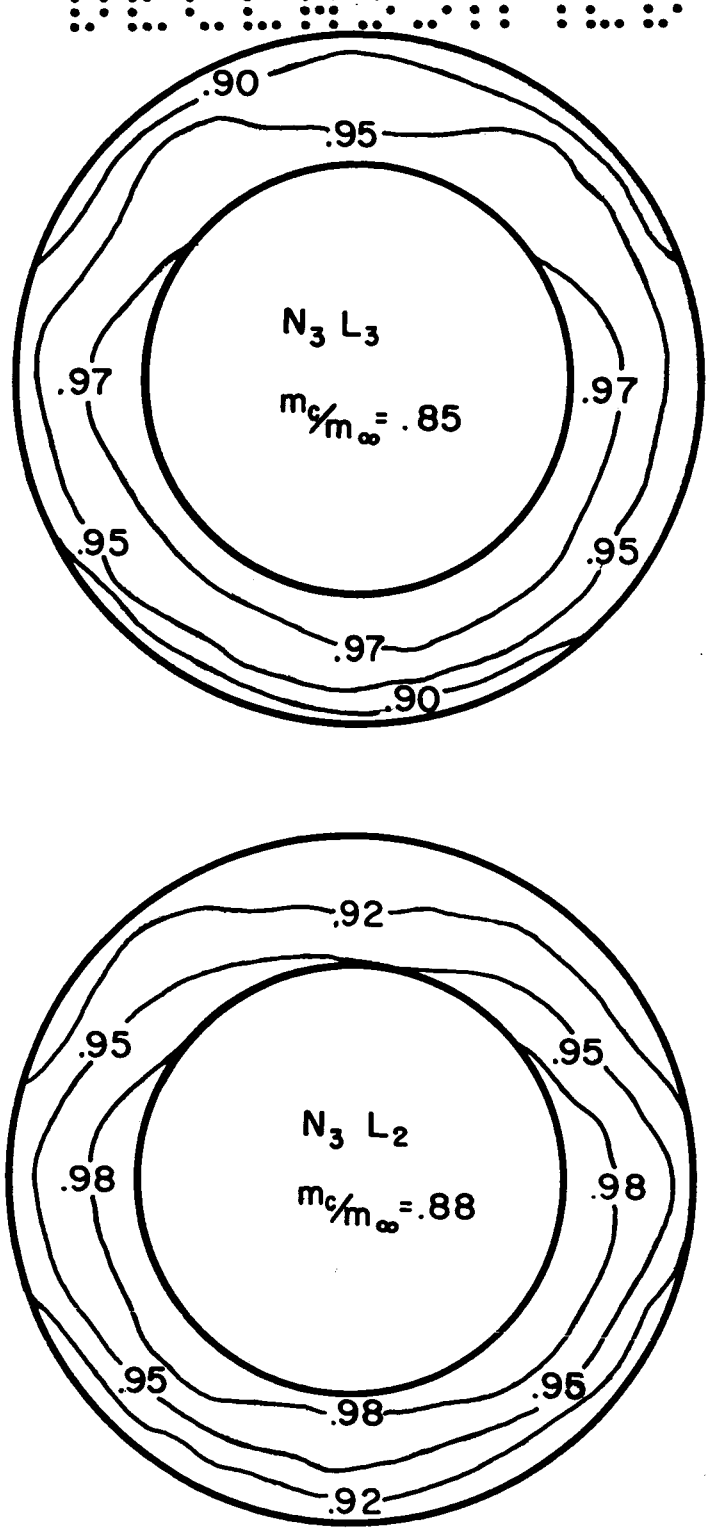

Figure 18.- Typical total-pressure distribution at the compressor station; $M_\infty = 1.5$; $\alpha = 3.0^\circ$.

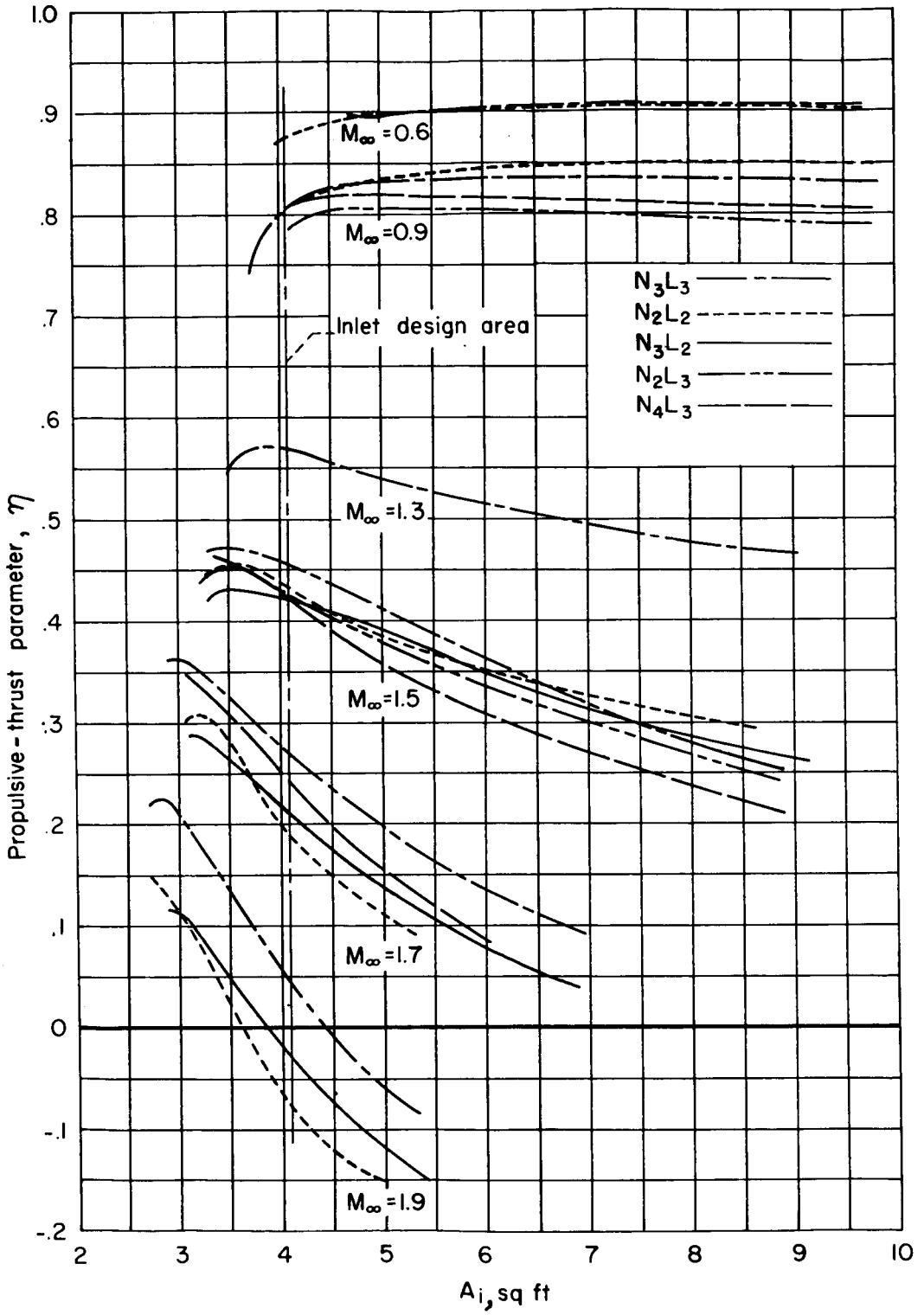

Figure 19.- Propulsive efficiency as a function of inlet area for the five most favorable inlet combinations; altitude = 35,000 ft.

[redacted]